

AD-A151 750

STIMULATED BRILLOUIN SCATTERING REFLECTIVITY IN THE
PRESENCE OF VARIOUS ABERRATORS(U) AIR FORCE INST OF
TECH WRIGHT-PATTERSON AFB OH SCHOOL OF ENGI.

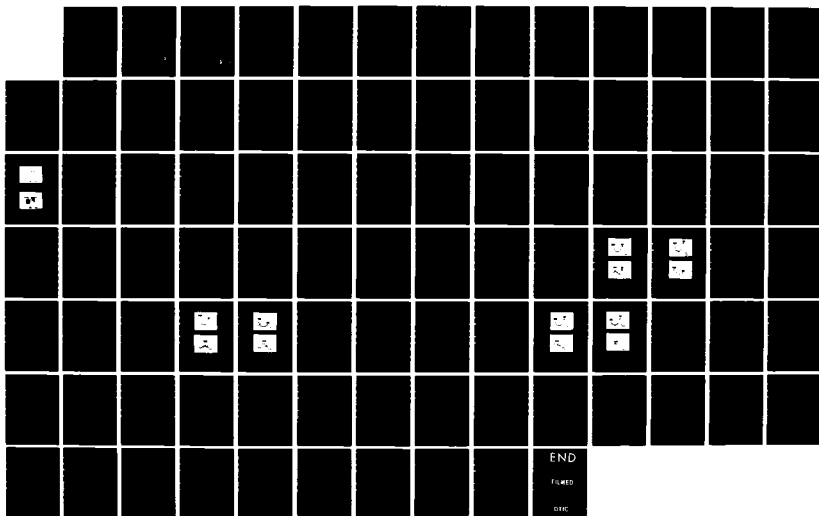
1/1

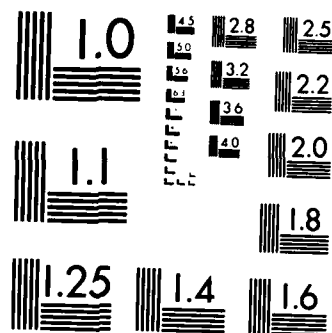
UNCLASSIFIED

T F LOWUM DEC 84 AFIT/GE/PH/84D-1

F/G 20/5

NL

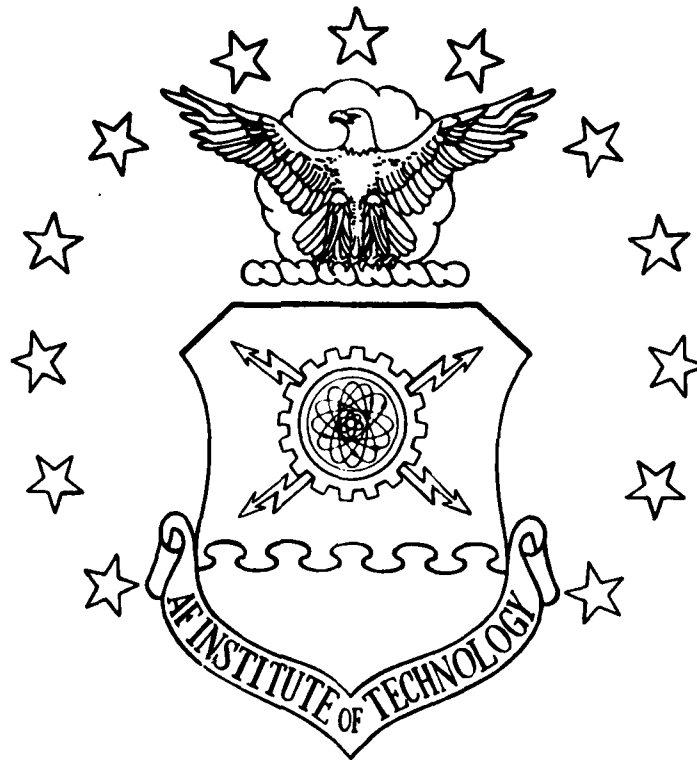




MICROCOPY RESOLUTION TEST CHART
NATIONAL BUREAU OF STANDARDS-1963-A

①

AD-A151 750



STIMULATED BRILLOUIN SCATTERING REFLECTIVITY
IN THE PRESENCE OF VARIOUS ABERRATORS
THESIS

Thomas F. Lowum
Second Lieutenant, USAF
AFIT/GE/PH/84D - 1

DTIC FILE COPY

DTIC
MAR 28 1985

DEPARTMENT OF THE AIR FORCE
AIR UNIVERSITY
AIR FORCE INSTITUTE OF TECHNOLOGY

Wright-Patterson Air Force Base, Ohio

85 03 13 155

STIMULATED BRILLOUIN SCATTERING REFLECTIVITY
IN THE PRESENCE OF VARIOUS ABERRATORS
THESIS

Thomas F. Lowum
Second Lieutenant, USAF

AFIT/GE/PH/84D - 1

Accession For	
NTIS GRA&I	<input checked="" type="checkbox"/>
DTIC TAB	<input type="checkbox"/>
Unannounced	<input type="checkbox"/>
Justification	
By	
Distribution/	
Availability Codes	
Dist	Avail and/or Special
A-1	



DTIC
ELECT
S MAR 28 1985 **D**

AFIT/GE/PH/84D-1

STIMULATED BRILLOUIN SCATTERING REFLECTIVITY IN
THE PRESENCE OF VARIOUS ABERRATORS

THESIS

Presented to the Faculty of the School of Engineering
of the Air Force Institute of Technology
Air University
In Partial Fulfillment of the
Requirements for the Degree of
Master of Science in Electrical Engineering

Thomas F. Lowum, B.S.
Second Lieutenant, USAF

December 1984

Approved for public release; distribution unlimited

Preface

The purpose of this thesis was to characterize the nature of a light wave reflected by Stimulated Brillouin Scattering. The ability of the phase-conjugated wave to compensate for various types of aberrations was the specific question under study; this topic is of considerable interest, since SBS could provide a solution to the limits on system performance created by imperfect lenses, the fluctuations in the atmosphere, etc.

I would like to acknowledge the complete support of AFWAL/AADO in carrying out this experiment. I would especially like to thank J. Brandelik and D. Smith for spending much of their valuable time giving me much-needed tutoring, guidance, and advice. The support of my thesis advisor, Dr. W.B. Roh, was also greatly appreciated.

Table of Contents

	page
Preface	ii
List of Figures	v
List of Tables	vii
Abstract	viii
 I. Introduction	 1
Background	1
Problem Definition	1
Approach	2
Presentation	2
 II. Theory	 4
Overview of the Process	4
Influence of Spectral Linewidth and Interaction Length on SBS	 6
Properties of the Phase-Conjugate Wave	7
 III. Experimental Setup and Equipment	 11
Characterization of Laser	13
Laser Output Power	15
Beam Divergence	15
Spot Size	15
Coherence Length	15
Linewidth	15
Temporal Pulse Shape	16
Polarization Analyzer	16
Beam Splitters	18
 IV. Experimental Measurement of SBS Reflectivity	 19
Cell Description and Reflectivity	19
Aberrators Displaying Birefringence	27
Cornu Pseudodepolarizer	27
Sapphire Quarter-Wave Plate	28
Aberrators Displaying Lensing Effects	29
Cylindrical Lens Telescope	31
Single Cylindrical Lens	34
One-Dimensional Apertures	36

Two-Dimensional Apertures	43
Large Screen	44
Fine Screen	47
Miscellaneous Aberrators: 50% Beam Splitter	50
V. Problems, Conclusions, and Recommendations	57
Problems Encountered During Experimentation	57
Energy Meters	57
Laser	57
Beam Splitters	57
Mounting Hardware	58
Interferometer	58
Conclusions	60
SBS Cell Performance	60
Correction for Birefringent Aberrators	61
Correction for Focusing Aberrators	61
Correction for 1-D and 2-D Apertures	61
Recommendations for Further Study	61
Tapered Waveguide SBS Cell	61
Investigation of Cornu Pseudodepolarizer . .	62
Interferometer	62
Appendix A: Beam Splitter Reflectivity	64
Appendix B: Derivation of Interferometer Method for Measuring Phase Conjugation Quality	67
Bibliography	76
Vita	79

List of Figures

Figure	Page
2.1 Phase-Conjugate Reflection vs Specular Reflection	8
2.2 Wavefront Reproduction by SBS	9
3.1 Experimental Setup	12
3.2 Schematic of Nd:YAG Laser Used in Experiment	14
3.3 Long-Pulse Temporal Characteristics	17
3.4 Q-Switched Temporal Characteristics	17
4.1 Normal SBS Cell and Capillary Cell	20
4.2 SBS Return vs Long-Pulse Laser Output for Capillary Cell	22
4.3 SBS Return for Q-Switched Laser Output - Capillary Cell	22
4.4 Correlation Between Long-Pulse Laser Output Variations and Variations in SBS Return	24
4.5 Correlation Between Q-Switched Laser Output Variations and SBS Return Variations	24
4.6 Temporal Shape of Long-Pulse SBS Return	26
4.7 Temporal Shape of Q-Switched SBS Return	26
4.8 Sapphire Quarter-Wave Plate Sliding Into Beam	30
4.9 Energy vs Position of Sapphire Plate in Beam	30
4.10 SBS Return vs Magnification of Cylindrical Telescope . .	32
4.11 Focal Spot from Cylindrical Telescope	34
4.12 Construction of One-Dimensional Apertures from Overlapping Microscope Slides	37
4.13 SBS Energy vs Output Energy - 7 Aperture Stack	38
4.14 Mirror Return Energy vs Output Energy - 7 Aperture Stack	40
4.15 Spatial Distribution of Return Pulse with 7 Aperture Stack at Near-Field Point	41
4.16 Spatial Distribution of Return Pulse with 7 Aperture Stack at Far-Field Point	42
4.18 Large Screen	44
4.19 SBS Energy vs Input Energy - Large Screen	45
4.20 Mirror Retro Energy vs Input Energy - Large Screen . . .	46
4.21 Spatial Distribution of Return Pulse with Large Screen in Near Field	48
4.22 Spatial Distribution of Return Pulse with Large Screen in Far Field	49
4.23 50% Beam Splitter	50

4.24	SBS Energy vs Input Energy - 50% Beam Splitter	52
4.25	Mirror Return Energy vs Input Energy - 50% Beam Splitter	53
4.26	Spatial Distribution of Return Pulse with 50% Beam Splitter at Near Field Point	54
4.27	Spatial Distribution of Return Pulse with 50% Beam Splitter at Far Field Point	55
5.1	Interferometer Used to Measure Phase Conjugation Quality	58
A.1	Orthogonal Polarization Components	64
B.1	Interferometer for Phase Conjugation Measurements	67
B.2	First Surface Reflection from Beam Splitter	68
B.3	Second Surface Reflection from Beam Splitter	68
B.4	Phase Shift Between Paths Going to Meter M2	69
B.5	Phase Shift Between Paths Going to Meter M1	69
B.6	Fringes at Meter M1 Resulting from Interferometer	74
B.7	Interference Fringes with Bias Term Removed	75

List of Tables

Table		Page
I.	Transmissions of Various Focal-Length Cylindrical Lenses	33
II.	Beam Splitter Reflectivity vs Polarization Angle of Incident Light	65
III.	Energy Meter Correction Factor vs Polarization Angle of Incident Light	66

Abstract

The phase-conjugate nature of a light wave reflected by Stimulated Brillouin Scattering was studied to determine the amount of compensation for aberrations that SBS could provide. The SBS medium used was CS_2 liquid contained in a cylindrical glass cell. Two different types of cell were used: one with a narrow capillary waveguide inside it and another without any waveguide.

The ability of SBS to correct for aberrators which change the polarization of the beam, focus the beam, or diffract the beam were studied. These included a sapphire quarter-wave plate, a Cornu Pseudodepolarizer, a cylindrical lens telescope, a single cylindrical lens, overlapping microscope slides (one-dimensional apertures), and a piece of wire mesh (two-dimensional apertures).

A solid state Nd:YAG Q-Switched laser was used as the light source. Two EG&G Model 580 radiometers measured the energy in the laser output pulse and the reflected pulse. A linear, 1000-element diode array connected to an oscilloscope displayed the spatial distribution of both pulses.

The Q-switched output of the laser caused plasma breakdown in the liquid, which adversely affected the SBS return. The data on the SBS return when the laser was Q-switched was too inconsistent to draw conclusions from. When the laser was run un-Q-switched, the data was much more consistent.

The SBS return, when the laser was running long-pulse, compensated either partially or completely for all of the aberrators in the system. The results also indicated that the cell with the waveguide had a much lower SBS threshold than the cell without the waveguide. Finally, recommendations for further study on the effects of the Cornu Pseudodepolarizer, on a way to measure phase-conjugation quality, and on a tapered-waveguide cell were given.

Stimulated Brillouin Scattering Reflectivity in the Presence of Various Aberrators

I. Introduction

Background.

Stimulated Brillouin Scattering is a nonlinear optical process in which a light wave incident on a transparent medium, such as a liquid or a gas, is backscattered by the creation of an acoustic wave in the medium. The backscattered wave has the property of being phase-conjugate to the incident wave.

A way to visualize the concept of a phase-conjugate wave is to imagine watching a movie of a rock being thrown into a quiet pond. The waves traveling outward from the point where the stone hits the water represent the light waves incident on the transparent SBS medium. If the film was played backwards, the ripples in the pond would appear to travel backward to the stone's impact point; The waves would retrace their path of travel back to their origin. This backward-filmed version of the ripples represents the backscattered phase-conjugate light wave.

The phase-conjugate light wave behaves just like the ripples in the pond when the film plays backwards. For this reason, a phase-conjugate light wave is often referred to as a time-reversed light wave. Zel'Dovich, et al. (29) found in 1972 that a PC light wave could correct for any phase distortions in a double-pass configured optical system. When the backward traveling light wave passed back through the source of the phase distortion, it compensated for the distortion it underwent on the first pass. Much experimental and theoretical investigation of phase distortion correction has occurred since then, but much less investigation of diffraction or polarization aberrations has taken place.

Problem Definition

The objective of this thesis is to experimentally characterize the SBS reflection occurring in CS_2 liquid. The SBS reflectivity is

measured with various phase, polarization, and diffraction aberrators placed in the system. The spatial distribution, temporal characteristics, and energy of the retro-reflected SBS pulse are also measured.

Approach

A double-pass optical configuration was set up and aligned; all equipment for the experiment was supplied by AFWAL/AADO. Using a Nd:YAG laser, the reflectivity of the CS₂ cell was measured in the presence of the various aberrators. Measurements were also taken with a regular flat mirror replacing the SBS cell, so that the two types of reflections (specular and SBS) can be compared. EG&G model 580 radiometers measured the energy and temporal characteristics of the laser output pulse and return pulse. A 1000- element linear diode array displayed the spatial distribution of the pulses.

Presentation

Elementary background theory on SBS is presented in Chapter II. This includes some theory on how SBS occurs and a discussion of the interesting aspects of the phase-conjugate wave.

Chapter III contains a description of the experimental set up. Each component used in the experiment is described in detail. The Nd:YAG laser is characterized in terms of its output pulse energy, temporal shape, spatial distribution, linewidth, coherence length, and beam divergence. Calibration of the measuring instruments and special characteristics of the components in the system are discussed.

Chapter IV contains the experimental results. The first section contains measurements of cell reflectivity without any aberrators present. This is done to provide a basis of comparison for SBS performance with aberrations placed in the system to cell performance without any aberrations. After the SBS cell has been characterized, measurements are taken with the aberrators in place.

The first aberrators investigated are those displaying birefringence effects. In this way, the effects of changing the beam's polarization are examined.

where

f = linewidth in Hz

c = speed of light

d = etalon mirror separation

l_3 = FWHM width of a fringe on the array

l_1 and l_2 = the distances between two adjacent fringes on the array. Two measurements of this distance are taken and averaged.

The linewidth for Q-switched output is 10.56 GHz and for long pulse is 7.92 GHz.

Temporal Pulse Shape. The temporal characteristics of the laser were determined by looking at the external output of the EG&G radiometer. Figure 3.3 shows the temporal shape of the long-pulse output. The laser emits many small spikes, each lasting about .5usec. The entire series of spikes lasts about 175 usec.

Figure 3.4 shows the Q-switched temporal characteristics. The laser output still consists of several spikes, but each of these spikes has more energy than the long-pulse spikes and has a FWHM width of 20 nsec. The series of Q-switched spikes lasts about 60 usec.

The long-pulse output has more total energy than the Q-switched output, but since the Q-switched pulse is much shorter, it has much higher peak power. According to equation (13), the SBS amplification is proportional to peak power (or intensity). This means that the Q-switched output will reach SBS threshold at a lower total energy level than the long pulse output will.

Polarization Analyzer

The polarization angle of the laser output can be controlled by placing a rotatable polarization analyzer in the beam, just before the beam expander. This analyzer, consisting of a calcite cube polarizing beamsplitter, lets through only that portion of the laser pulse which has polarization matching the analyzer axis. The analyzer axis can be rotated, so that the direction of polarization passing through the analyzer can be controlled. Since the laser output is horizontally

Laser Output Power. The output energy of the laser was measured using a Laser Precision Model 7200 Energy Meter; the laser's output energy could be varied from 1.5 mJ to 13 mJ. For a given voltage setting on the laser, the laser's Q-switched output is about 0.5 mJ less than the long-pulse output.

Beam Divergence. To measure the divergence of the output beam, a variable aperture was placed at the focus of a 2.8m converging lens. Measurements were taken of the energy going through the aperture vs aperture diameter; the aperture size which allowed 90% of the energy through gave the focal spot size. The value of 90% was chosen as approximately equal to the $1/e^2$ value of the beam energy. After finding the focal spot size, beam divergence was calculated from $\theta = D/f$. The beam divergence, after the beam has been through the 5x expander, is .091 milliradians.

Spot Size. The spot size of the enlarged, collimated beam was measured in a way similar to the beam divergence measurement. An aperture was put into the beam and closed down until only 90% of the maximum energy got through it. The diameter of the spot is $2w_0 = 1.143$ cm.

Coherence Length. The coherence length of the laser was determined by putting two partially reflecting mirrors ($R = 0.85$ and $R = 0.95$) in the beam, overlapping their reflections, and observing the resulting interference fringes on the diode array. As the mirror separation gradually increased, the interference fringes became less visible. The coherence length is equal to the maximum mirror separation before the fringes wash out completely. This was measured as $l_c = 45$ cm for both Q-switched and long pulse output.

Linewidth. The laser's linewidth was measured using a Fabry-Perot etalon. A 75mm diverging lens was placed in the beam at the entrance to the etalon, and a 1m converging lens was placed at the output of the etalon. The diode array was then placed in the focal plane of the 1m lens to observe the interference fringes. The linewidth was determined from

$$f = 1/3(c/2d)/.51_1 + .51_2 \quad (14)$$

beam size and the transverse modes running in the cavity. The front mirror is a flat mirror, with $R = .50$.

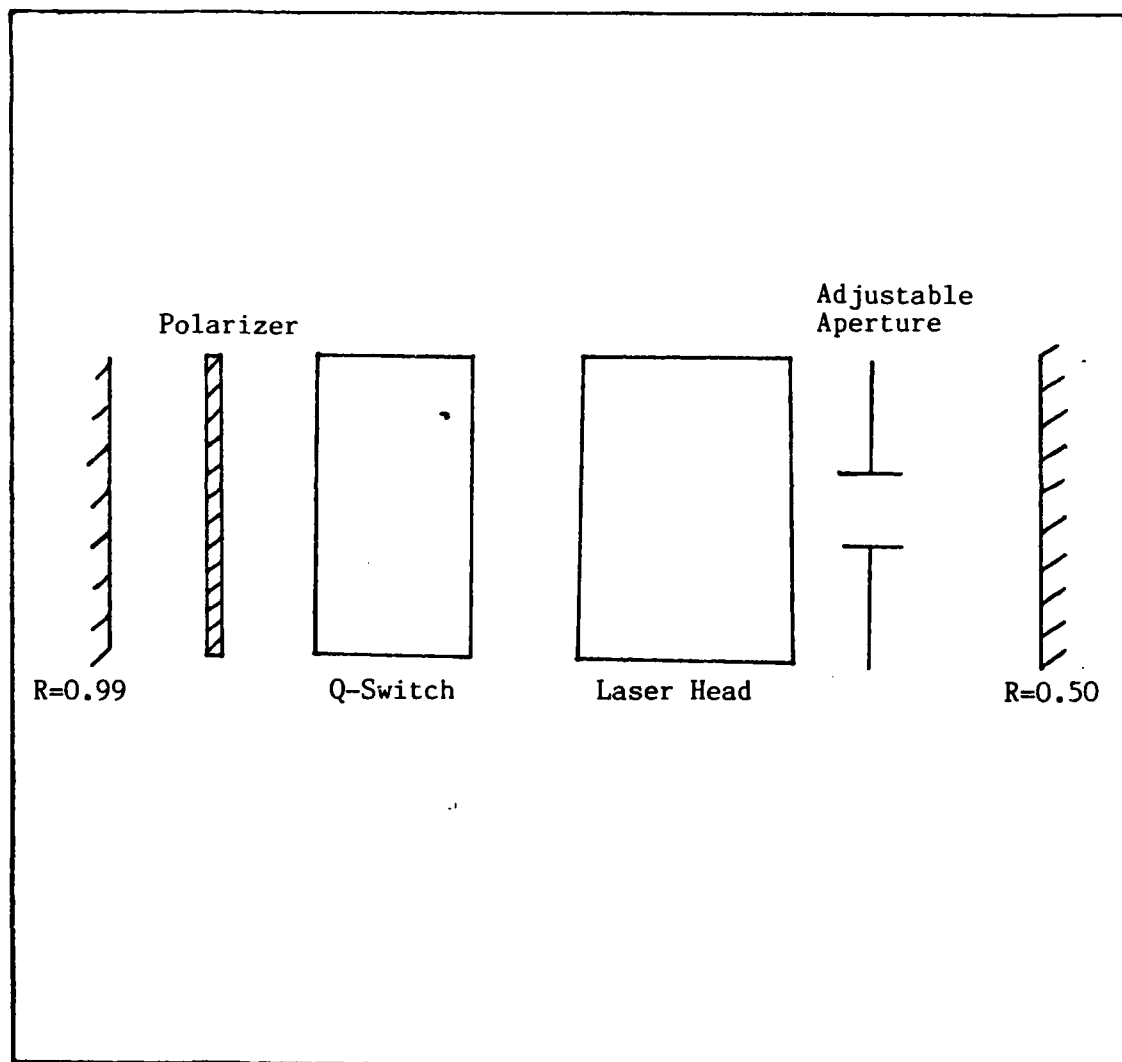


Figure 3.2 Schematic of Nd:YAG Laser Used in Experiment

L1 is a converging lens used to focus the beam into the SBS cell. Its focal length was varied during the experiment.

The SBS cell is a glass cell which contains the CS_2 liquid medium. The length of the cell and its shape are described in a later chapter.

M2 is an 85% reflecting mirror used to turn a sample of the reference beam toward the diode array. M3 is a 50% reflecting mirror used to turn a sample of the retro pulse toward the diode array, and also to let some of the reference beam sample pass through it to the array.

The linear, 1000 element diode array, viewed on the oscilloscope, showed the spatial distribution of the reference and retro pulses. The firing of the laser is triggered by the start of the array readout sweep, so that the laser pulse is synchronized with the array readout. Since the array is one dimensional (vertical), it gives the spatial information for only a thin vertical slice of the spot. The laser output is far from being spatially uniform, therefore the array output depends on exactly where the array slices through the spot. In most cases, the reference and retro spots were centered on the array. Very little quantitative information about the intensity of the pulses can be gained from the array, since neutral density filters often had to be put in front of the array to prevent its saturation. The array is one inch long, so all pictures of the array output are scaled in tenths of inches along the x-axis.

Points 1,2,3, and 4 are the places in the setup where aberrators could be inserted. Point 2 will be referred to as the "far field point", point 3 as the "near field point".

Characterization of Laser

The laser used in this experiment, shown in figure 3.2, was set up completely from lab components by Mr. Don Smith. It is a Nd:YAG laser operating at 1.06 μm . The back mirror is a flat mirror with $R = .99$. The dielectric polarizer polarizes the light in the horizontal plane. The electro-optical Q-switch is driven by a high voltage pulse generator. The laser head contains the YAG crystal, as well as the flash lamps. The adjustable aperture gives control over the output

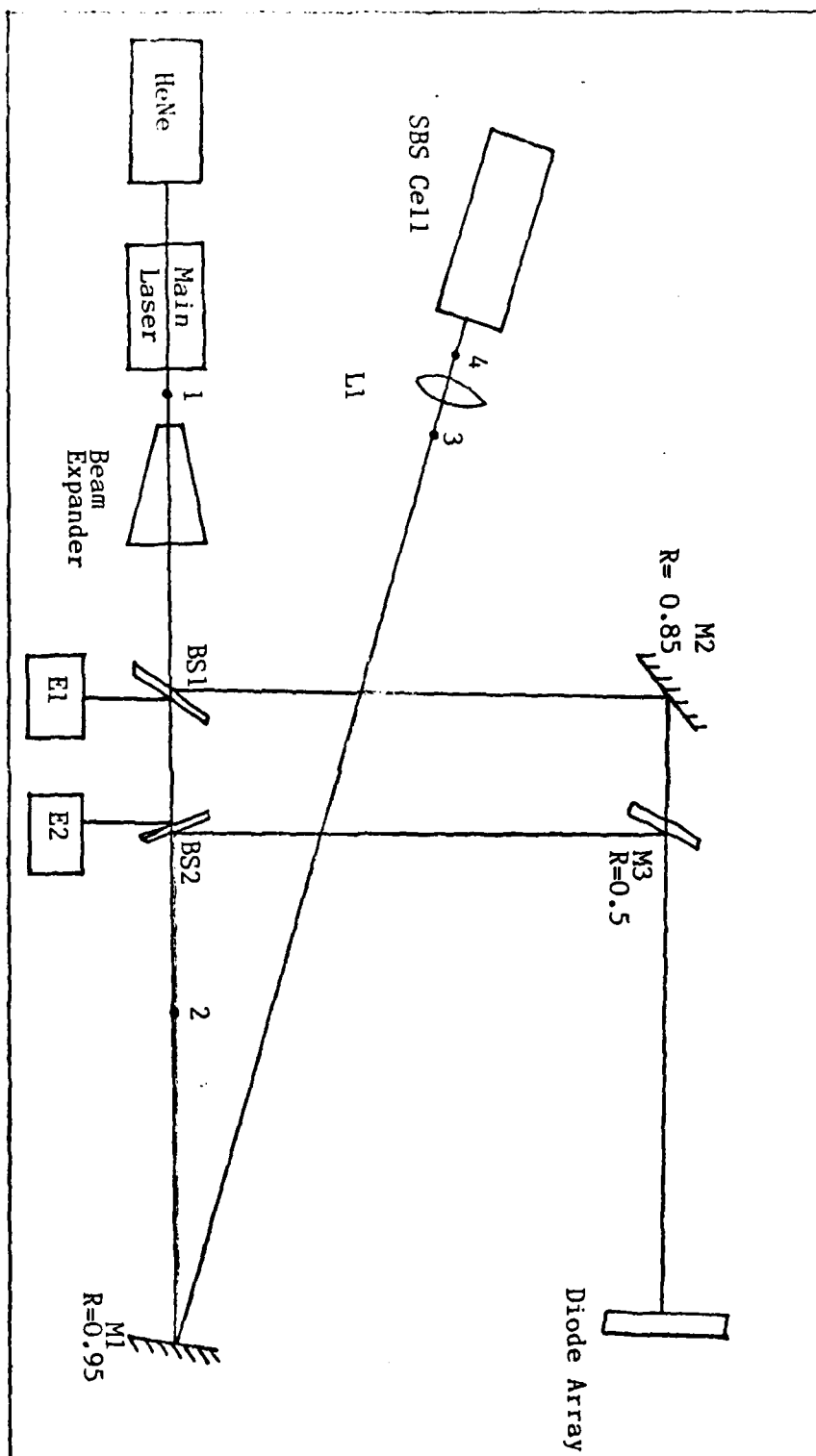


Figure 3.1 Experimental Setup

III. Experimental Setup and Equipment

This chapter provides a description of the setup used in this experiment. It provides a description of each piece of equipment used in this setup and any special characteristics of the equipment. Figure 3.1 shows the setup for the experiment. The HeNe laser is bore-sighted through the main laser and is used for alignment purposes. The main laser is a solid state Nd:YAG operating at 1.06 μm .

The beam expander consists of a diverging lens, with $f = 5\text{cm}$, and a converging lens, with $f = 25\text{cm}$. The separation between the two lenses is 20cm. This combination of lenses provides a 5x expansion of the input beam, and also collimates the beam.

BS1 is a beamsplitter used to send a sample of the reference beam (the output beam of the laser) to the diode array, and to send a sample of the retro beam (the backward travelling beam) to E2. BS2 is a beamsplitter used to send a sample of the retro beam to the array, and to send a sample of the reference beam to E1.

E1 and E2 are both EG&G Model 580 Radiometers. These meters are used for almost all of the energy measurements in the experiment, since they were the most sensitive meters available for use. Unfortunately, the EG&G meters had to be operated without their narrow beam adaptors on, since these cut down the intensity incident on the detector surface. Without the narrow beam adaptor in place, the reading on the EG&G depends on the position of the laser spot on the detector surface. This situation made the meters difficult to calibrate in real energy units and to maintain consistent energy readings. Every effort was made during the experiment to keep the spot on the center of the meter, keeping the energy readings as consistent as possible.

The external output of the EG&G meters also provided a way to look at the temporal shape of the reference pulse and the retro pulse. The external outputs of the EG&G meters were displayed on a Tektronix Storage Oscilloscope.

M1 is a 95% reflecting mirror used to turn the beam back down the table. This mirror was necessary due to space limitations on the table.

The phase-conjugated backscattered wavefront also reproduces the polarization state of the input wave (21:153). For high fidelity phase conjugation, the input wave must have linear or circular polarization (9:148). To see the need for a linearly polarized input wave, consider the case of an unpolarized input wave. As the wave enters the SBS medium, the dipoles in the medium try to align themselves with the fluctuating E field. If the input wave is unpolarized, the E field will be fluctuating in all different directions and the induced dipoles will not be able to align themselves with the E field. If, on the other hand, the input wave is linearly polarized, the induced dipoles will fluctuate along the line of the light's polarization and an acoustic wave suitable for SBS will be generated.

A final interesting aspect of the phase-conjugate wave is that of pulse compression. A short input pulse on the order of a few nanoseconds can be significantly depressed in time. This thesis does not deal with this aspect of SBS, so no explanation will be given for this occurrence.

difference between a normal reflection and a phase conjugate reflection (21:159).

The wavefront reproduction illustrated in figure 2.2 is the basis for the correction of phase aberrators by SBS, which was first verified by Nosach, et al., in 1972 (18). Since SBS compensates for all phase aberrations after passing back through them, the divergence of the reverse beam is very nearly diffraction limited (assuming that the input wave was a plane wave). Without this correction, the phase aberrations would significantly increase the beam's divergence.

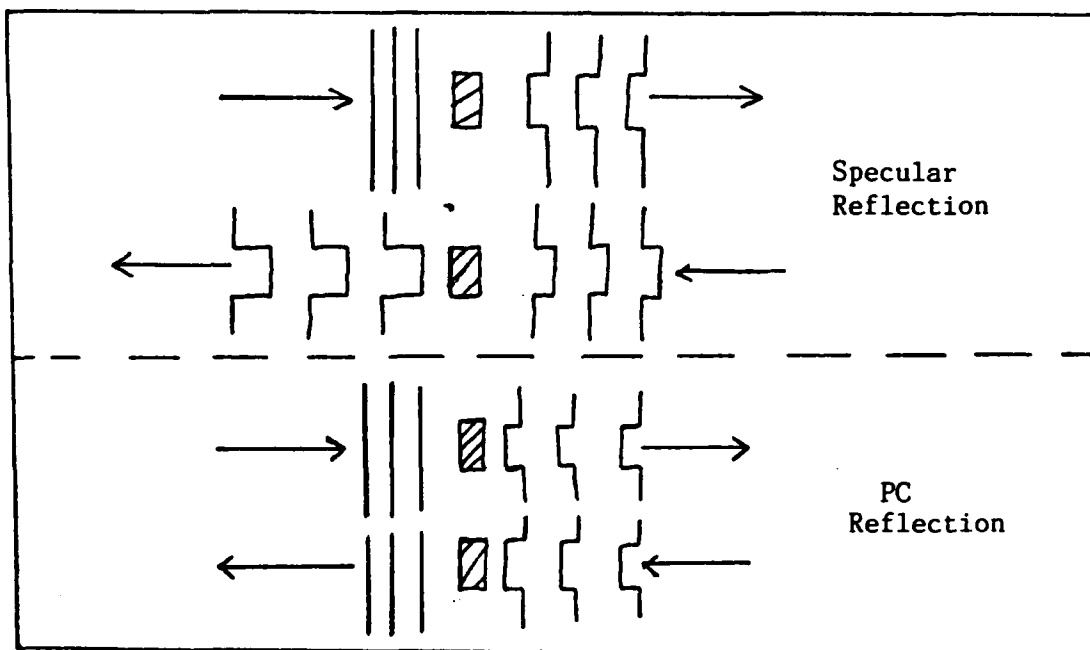


Figure 2.2 Wavefront Reproduction by SBS

standard mirror; Figure 2.1 shows this difference. Another interesting property of the phase-conjugate reflected wave is that it reproduces the phase front of the incident wave everywhere along its path. At any point along the path of the incident wave and the reverse wave(they will travel the same path), the phase fronts of both waves will be identical. This phase front reproduction means that any phase aberration in the beam's path will be compensated for after the reverse wave passes back through that aberration. If the phase of the backscattered wave exactly reproduces that of the incident wave, then the SBS wave must compensate for any aberration in its path in order to recreate the phase front of the incident wave. Figure 2.2 shows this

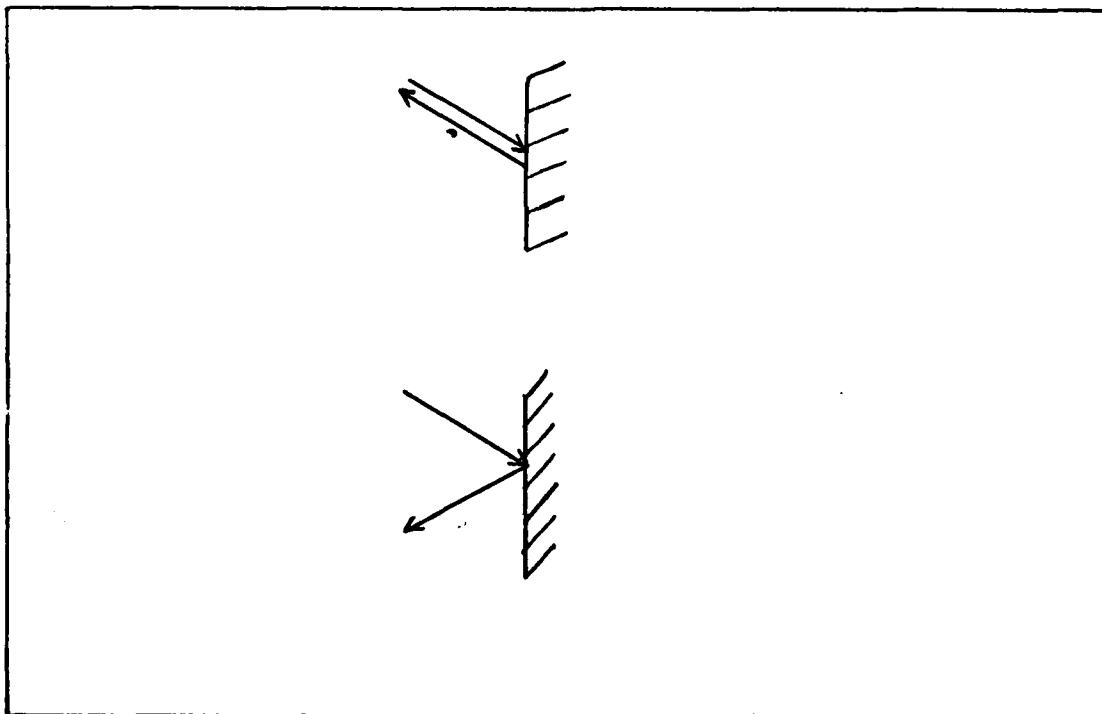


Figure 2.1 Phase-Conjugate Reflection (top) vs Specular Reflection (bottom)

and the pump laser linewidth ($\Delta\nu_p$). The Spontaneous Scattering Linewidth is a material-dependent parameter which gives a measure of the variations in the susceptibility due to entropy and pressure fluctuations in the medium. For SBS, $A = \gamma^2 L^2 / n^3 c \rho v$, where

γ = photoelastic constant of the medium

ρ = density of the medium

n = refractive index of the medium

$k = 2\pi/\lambda = 5.93 \times 10^4 \text{ cm}^{-1}$

c = speed of light

v = speed of hypersound in medium.

For the purpose of this discussion, all factors determining A are assumed to be constants.

For CS_2 liquid, $\Delta\nu_{sp} = 21.2 \text{ MHz}$ (14:1115). Thus,

$$g = A / (\Delta\nu_p + 21.2 \text{ MHz})$$

and amplification is proportional to

$$\exp\{A I_1 L / (\Delta\nu_p + 21.2 \text{ MHz})\} \quad (13)$$

Equation (13) shows that as the pump laser's linewidth increases, the SBS amplification goes down substantially.

Equation (13) also reveals the influence of material breakdown on SBS gain. When the pump laser reaches a certain intensity, the structure of the SBS medium breaks down and a plasma forms. Since this plasma breakdown radically changes the structure of the medium, no SBS will occur in the medium behind the point where the plasma forms. The plasma breakdown effectively shortens the interaction length of the medium. From equation (13), the shortened interaction length L results in a lower SBS gain.

Properties of the Phase Conjugate Wave

The backward travelling SBS wave has many interesting properties arising from its phase-conjugate nature. The first notable property is that the backscattered wave exactly retraces the path of the incident wave. This differs greatly from a specular reflection off of a

v_s = velocity of sound in the medium

The three above equations show how the electrostrictively generated accoustic wave couples the incident and reflected light waves together. The accoustic wave, given by Eq (7), is generated by the electrostrictive forces in the medium, and is therefore related to the nonlinear induced dipole moment given by Eq (5).

Equations (6), (7), and (8) show that the accoustic wave couples the reflected and incident waves to the density fluctuations in the medium. Solution of this set of coupled equations reveals that the backscattered mode with the highest gain is phase-conjugate to the input wave:

$$E_1 = \text{Re}[\Psi(x,y)\exp\{if_1t - ik_1z\}] \quad (9)$$

$$E_{\text{SBS}} = \text{Re}[\Psi^*(x,y)\exp\{i(f_1 - f_s)t + ik_2z\}] \quad (10)$$

The value of f_s , the frequency of the accoustic phonons, is many orders of magnitude less than the optical frequency of the incident light wave, so the frequency shift of the reflected light wave may be ignored. For CS_2 liquid, the value of f_s is 5.85 GHz (14:1115). Ignoring this small frequency shift, Eq (10) may be rewritten as

$$E_{\text{SBS}} = \text{Re}[\Psi^*(x,y)\exp\{if_1t + ik_1z\}] \quad (11)$$

Influence of Spectral Linewidth and Interaction Length on SBS.

The solutions to Equations (6), (7), and (8) show that the magnitude of the backscattered wave increases exponentially, starting from noise level (8). The amplification of the backscattered wave is proportional to $\exp(gI_1L)$, where

I_1 =intensity of incident radiation in MW/cm^2

L =length of active medium in cm

and the gain g is

$$g = A/2\pi (\Delta\nu_p + \Delta\nu_{sp}) \quad (12)$$

The gain factor g depends on the spontaneous scattering linewidth ($\Delta\nu_{sp}$)

where χ = susceptibility. The nonlinear processes, such as SBS and Stimulated Raman Scattering, arise from the third order term of the nonlinear susceptibility .

When an intense light wave enters an SBS medium, the induced dipoles in that medium try to align themselves with the variations in the incident electric field. This electrostrictive force (tension/unit area) causes fluctuations in the density of the medium, and therefore generates accoustic phonons. If the group velocity of the resultant accoustic wave matches the group velocity of the incident light wave, the two waves will travel in step. Since the susceptibility (and the refractive index) of the medium depends on the medium's density, the accoustic wave scatters the incoming light by acting as a diffraction grating. A set of coupled differential equations may be written for the three waves in the medium - the incident light wave, the accoustic wave, and the reflected light wave.

$$\frac{d^2 E(f_1)}{dz^2} = n^2/c^2 \frac{d^2 E(f_1)}{dt^2} - 2\gamma/c^2 \rho_0 \frac{d^2}{dt^2} [\rho(f_s) E(f_2)] \quad (6)$$

$$\frac{d^2 \rho(f_s)}{dz^2} = 1/v_s^2 \frac{d^2 \rho(f_s)}{dt^2} - \gamma/2v_s^2 \frac{d^2}{dt^2} [E(f_1) E(f_2)] \quad (7)$$

$$\frac{d^2 E(f_2)}{dz^2} = n^2/c^2 \frac{d^2 E(f_2)}{dt^2} + 2\gamma/c^2 \rho_0 \frac{d^2}{dt^2} [\rho(f_s) E(f_1)] \quad (8)$$

where

$E(f_1)$ = incident light wave at frequency f_1

$\rho(f_s)$ = accoustic wave at frequency f_s

$E(f_2)$ = reflected light wave at frequency $f_2 = f_1 - f_s$

n^2 = normal value of dielectric constant in medium

γ = coefficient of electrostriction which relates the dielectric constant of the medium to the density of the medium: $\gamma = 0.5 \rho \, d\epsilon/d\rho$

ρ_0 = average density of the medium

II. Theory

Stimulated Brillouin Scattering is a nonlinear process in which an intense laser beam entering a clear medium is backscattered by the generation of acoustic phonons. Since this thesis is primarily experimental in nature, a complete theoretical treatment of this effect will not be presented. Enough of the theory will, however, be presented to provide sufficient understanding of the experimental procedures and results. The following treatment was taken from Ref(1) and Ref (14); for more detail about the theory behind SBS, refer to these texts.

Overview of the Process

The induced dipole moment (dipole moment/unit volume) of an isotropic medium, such as a liquid or a gas, can be expressed as a function of the electric field vector E:

$$P(E) = \epsilon_0[\epsilon_r(E) - 1]E \quad (1)$$

The permittivity term ϵ_r , which is nonlinear, can be expanded in the Taylor series

$$\epsilon_r(E) = [\epsilon_r^{(1)} + \epsilon_r^{(2)}E + \epsilon_r^{(3)}E^2 + \dots - 1] \quad (2)$$

In an isotropic medium, the term $(\epsilon_r^{(2)}E) = 0$. Therefore, the polarizability can be expressed as

$$P(E) = \epsilon_0[\epsilon_r^{(1)} + \epsilon_r^{(3)}E^2 + \dots - 1]E \quad (3)$$

The terms of order 4 or higher can be neglected, since

$$(\epsilon_r^{(n+1)} / \epsilon_r^{(n)}) < 10^{-6}$$

Using this approximation, the polarizability may be written as

$$P(E) = \epsilon_0[\epsilon_r^{(1)} + \epsilon_r^{(3)}E^2]E \quad (4)$$

or

$$P(E) = \epsilon_0[\chi^{(1)} + \chi^{(3)}E^2]E \quad (5)$$

Following this, aberrators having lensing or focusing effects are investigated. The degree of correction for the beam divergence introduced by the focusing element is determined.

The next section contains measurements taken in the presence of one-dimensional apertures. These apertures introduce diffraction into the beam. The following section extends this idea to two-dimensional apertures.

The final section, entitled "miscellaneous aberrators", looks at the cell reflectivity in the presence of a special 50% beam splitter.

Chapter V presents the conclusions drawn from the data. Problems which arose during the experiment and affected the results are discussed. Finally, recommendations for further study are presented.

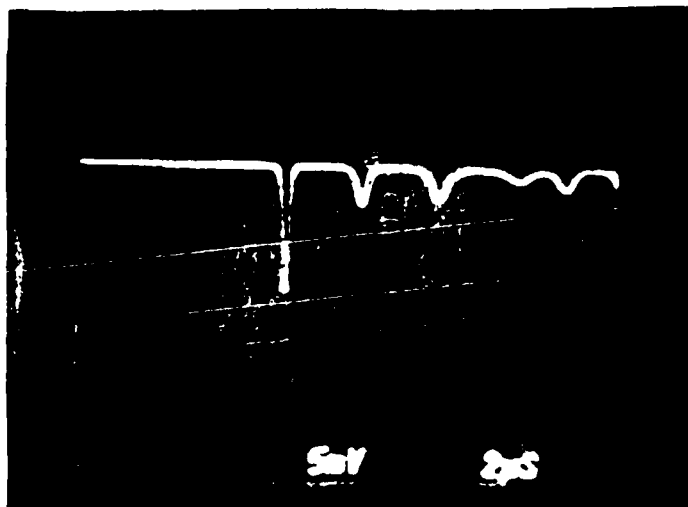


Figure 3.3 Long-Pulse Temporal Characteristics
(Horizontal Scale is 2μsec/div)

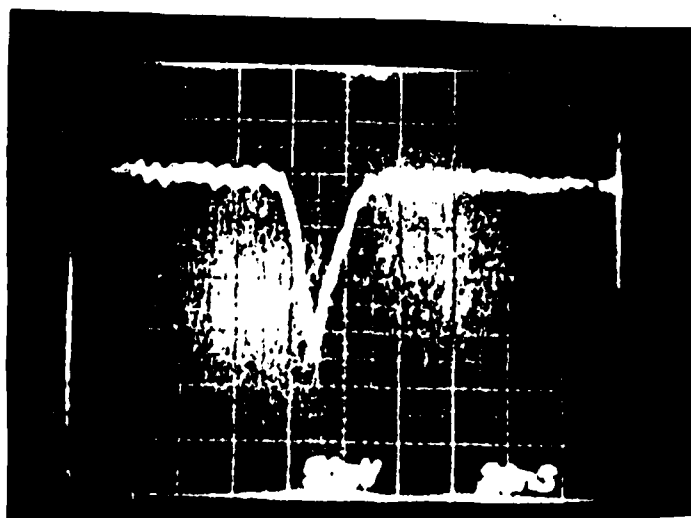


Figure 3.4 Q-Switched Temporal Characteristics
(Horizontal Scale is 20 nsec/div)

polarized, maximum throughput occurs when the analyzer is set at 0 degrees and minimum energy passes through with the analyzer at 90 degrees. This analyzer gives control over energy throughput, as well as polarization angle.

Beam Splitters. The beam splitters, used throughout the setup to split off portions of the reference and retro pulses, are uncoated, flat pieces of glass. The reflectivity of these beamsplitters depends on the polarization angle of the incident light.

Assuming that the refractive index for the beamsplitter is $n = 1.5$, the reflectivity for vertical polarization is $R = .09$ (this assumes that the beam splitter is at a 45 degree angle to the incident light). For horizontally polarized light, $R = .008$ (12:511). The reflectivity varies between these two values, depending on the polarization angle of the incident light. Appendix A gives more detail on these reflectivity calculations. Since the beam splitter reflectivities vary with polarization, all of the EG&G radiometer readings had to be corrected for the polarization of the reference beam. Appendix A gives the correction factors for various polarization angles.

Since the beam splitters have no anti-reflective coatings, each beam splitter has two reflections associated with it: one from the front surface and one from the back surface. The reflection from the front surface was the one used for measurements. The other reflected spot was easily apertured out, since the two spots were separated by several millimeters.

IV. Experimental Measurement of SBS Reflectivity

This chapter discusses the experimental measurement of SBS cell reflectivity in the presence of different aberrators. First, the reflectivities of the two different SBS cells used in this experiment are measured, and some characteristics of the two cells are discussed. Next, the effects of aberrators having some kind of birefringence effects are discussed. Following that, aberrators having lensing (focusing) effects are discussed. Next, one-dimensional and two-dimensional apertures are studied. Finally, the effects of a "miscellaneous" aperture are examined. All data points given in this chapter are the average of five laser pulses, unless otherwise noted.

The output energy of the laser, measured with the Laser Precision meter after the beam splitters, can be corrected to represent the energy at the cell entrance by taking into account the losses on the way to the cell:

$$E_{in} = (E_o)(R_{M1})(T_{aberrator})(T_{lens}) \quad (15)$$

$$E_{in} = (E_o)(.95)(.918)(T_{ab}) = .872T_{ab}E_o$$

The retro pulse energy, read on the EG&G meter, can be corrected to give the value of the energy coming out of the cell:

$$E_{sbs} = kE_m / (T_{lens})(T_{ab})(R_{M1}) \quad (16)$$

$$E_{sbs} = .425E_m / T_{ab}$$

where k is a constant to convert the meter reading to mJ ($k = 0.37$).

The SBS reflectivity of the cell may be found by dividing equation (16) by equation (15):

$$R_{sbs} = .487E_m / E_o (T_{ab})^2 \quad (17)$$

Cell Description and Reflectivity

Figure 4.1 shows drawings of the two different SBS cells used in this experiment. The first cell (cell A) is a pyrex cylinder 35 cm in length and 2.5 cm in diameter. Windows of 0.5 cm thickness are cemented onto both ends of the cylinder. An opening at the top of the

cell, used to fill it with liquid, is sealed with a glass stopper.

Cell B is identical to cell A, except that it has a narrow capillary running down its center. This capillary, with a 1 mm bore diameter, acts as a waveguide for the incoming light. The narrow waveguide confines the light to a small space, bouncing it back and forth from the capillary walls. These bounces inside the capillary effectively increase the cell's interaction length, and therefore lowers the threshold for SBS to occur (see equation 13).

The alignment of the cell was critical to get a good SBS return. This alignment proved to present more of a problem with cell B than with cell A. The acceptance angle of the capillary waveguide is fairly small, so that the beam had to enter the capillary at a fairly precise angle in order to be contained inside it. The method used to align the cell was to gradually move it until the retro energy measured on the EG&G meter was maximized. The cell would usually have to be realigned each morning, since the clamps holding the cell in place would relax overnight. Realignment was also necessary every time the focusing

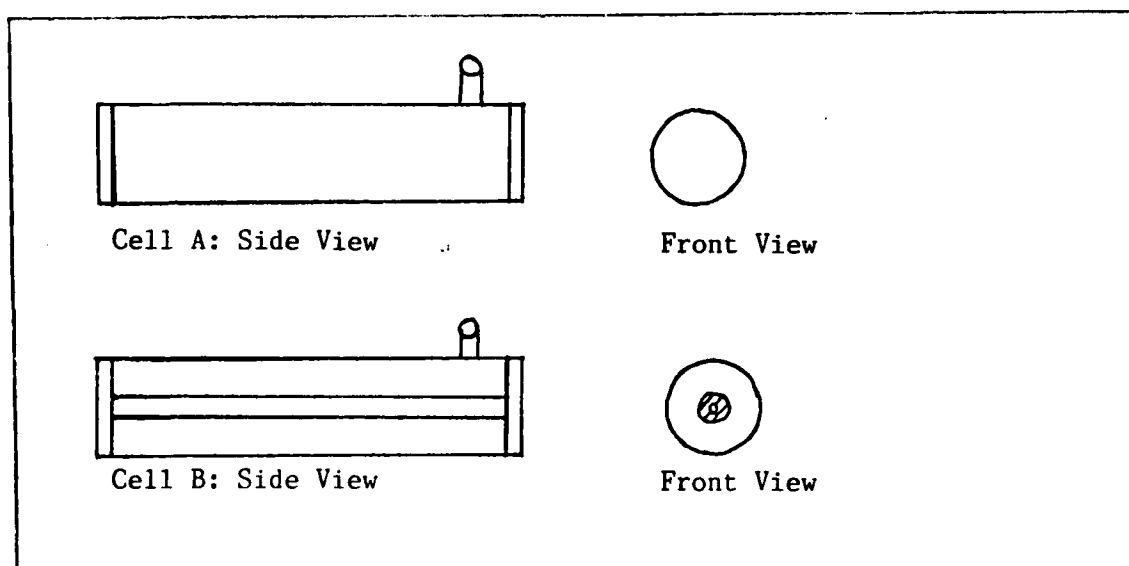


Figure 4.1 Normal SBS Cell (a) and Capillary SBS Cell (b)

lens was changed.

The reflectivities of both SBS cells used in the experiment were measured without any aberrators present. Several focal length lenses were tried in order to achieve the maximum SBS return. As the focal length of the focusing lens was changed, the focal spot size in the cell changed; the longer the focal length, the larger the spot. This changed the peak power density inside the cell. With both cells, the $f = 1\text{m}$ lens appeared to give the largest and most consistent returns. For this reason, it was used for most of the aberrator measurements.

The SBS return also varied greatly with the laser output. A long-pulse laser output resulted in a highly consistent SBS return. The retro pulse had the same energy and spatial distribution from pulse to pulse, within the variation of the laser output. Figure 4.2 shows the SBS return vs laser output for long pulse.

Unlike long-pulse, the Q-switched laser output often resulted in highly inconsistent and non-reproducible SBS returns. The retro pulses varied greatly, both in spatial distribution and in energy. When the laser was Q-switched, plasma breakdown often occurred in the SBS medium. This breakdown could effectively shorten the interaction length in the medium (see chapter II), and therefore lower the gain of the retro pulse. Since the peak power is much lower while running the laser long-pulse, no plasma breakdown occurs. Figure 4.3 shows the SBS energy vs laser output for Q-switched output. Note the increase in data variation (denoted by the error bars in the figure) over that for the long-pulse output.

The data shown in figure 4.2 and figure 4.3 were taken using the capillary cell (cell B). The data for Q-switched output with cell A shows even more variation than for the cell B case, while no SBS at all could be achieved with cell A using long-pulse output, due to cell A's higher SBS threshold. The SBS reflectivity for the capillary cell and long-pulse laser output, from Equation (17), is

$$R_{\text{sbs}} = .039$$

The SBS reflectivity for Q-switched output varied from 0.07 to 0.34.

In order to determine if the variation in the retro pulse energy

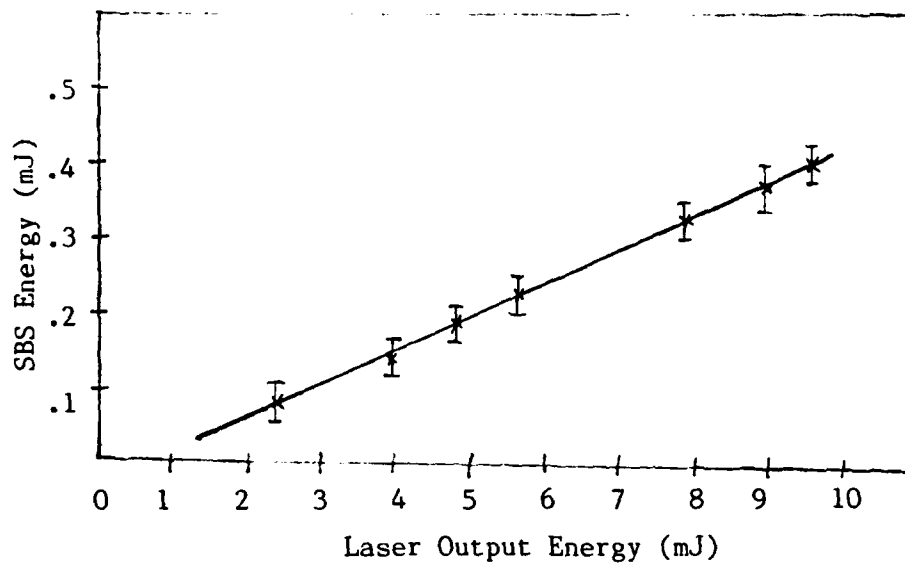


Figure 4.2 SBS Return vs Long-Pulse Laser Output for Capillary Cell

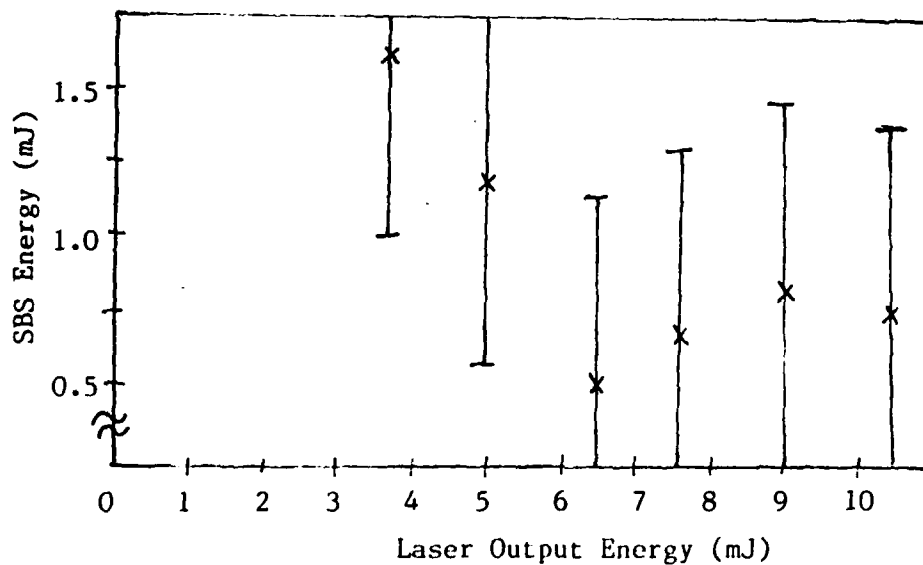


Figure 4.3 SBS Return vs Q-Switched Laser Output for Capillary Cell

had any correlation to the variation in the laser output, simultaneous energy measurements of the laser pulse energy and the retro pulse energy were taken. Figure 4.4 shows the correlation between the laser output and the SBS return for long pulse output. The changes in SBS energy correspond well to the changes in laser output energy from pulse to pulse.

Figure 4.5 shows the SBS energy vs Q-switched laser output. As the figure shows, there is little or no correlation between the pulse-to-pulse changes in SBS energy and the pulse-to-pulse changes in laser output energy. This leads to the conclusion that some other factor caused the large variations in the SBS return.

The inconsistent SBS return obtained with Q-switched laser output could also be a result of changing laser linewidth. As the laser power increases, the laser's linewidth could also increase. According to Equation (13), as linewidth increases, SBS amplification decreases. To determine if this was a problem, the energy going to the cell was controlled with the polarization analyzer.

The analyzer could be rotated to control its throughput, thus changing the amount of energy going to the cell without changing the laser output energy. After correcting the beam splitter reflectivities for the changing polarization angle (see Appendix A for the correction factors), the SBS energy vs input energy was plotted. The variation of the SBS energy data was not reduced by this method, which means that the cause of the inconsistent SBS returns was probably something else.

To determine if any of the laser energy was contributing to Stimulated Raman Scattering, an InSb detector was installed at the exit of the cell (the far end). A mirror with high reflectivity at 1.06 μm , but low reflectivity at the Raman-shifted wavelength of 1.144 μm (23:276) was placed in front of the detector. In this way, the 1.06 μm radiation passing through the cell was blocked, and only the Raman-shifted radiation reached the detector. The detector measured zero Raman-shifted radiation, so no SRS was occurring. If it was occurring, this would have been one explanation for the low SBS reflectivity of the cell.

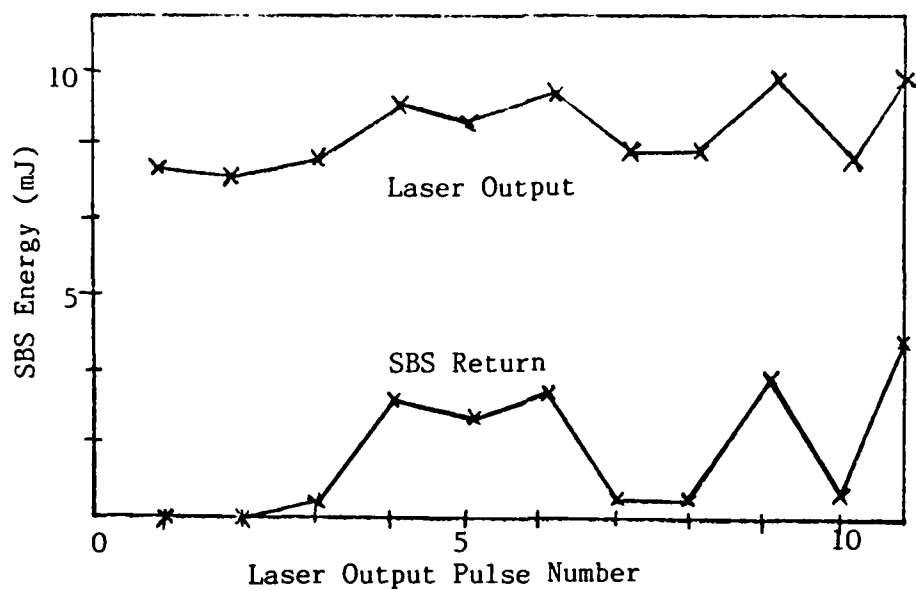


Figure 4.4 Correlation Between Long-Pulse Output Variations and Variations in SBS Return

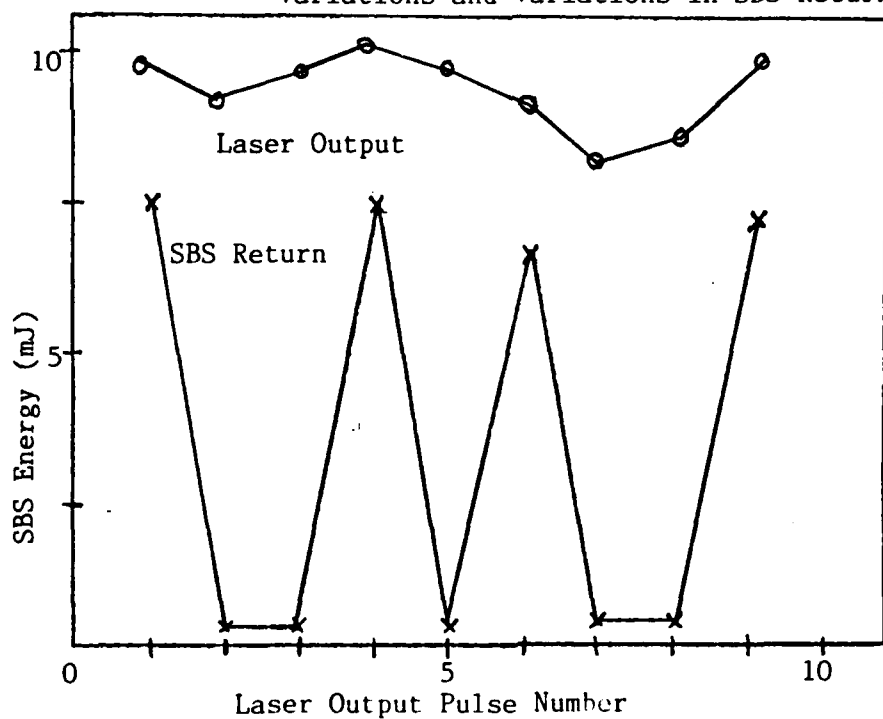


Figure 4.5 Correlation Between Q-Switched Laser Output Variations and SBS Return Variations

The temporal characteristics of the SBS pulse were also observed. Its temporal shape was similar to that of the laser output pulse. Figure 4.6 shows the temporal shape of the long pulse SBS return, while figure 4.7 shows the temporal shape of the Q-switched return. These can be compared to figures 3.4 and 3.5, which show the temporal shape of the long pulse laser output and the Q-switched output, respectively.

In the temporal profile of the Q-switched pulse (figure 4.7), the SBS pulse appears to be about 10 ns shorter than the laser output pulse. This is due to the transient behavior arising from the Q-switched pulse being shorter than the typical phonon lifetime (30 ns) in the CS_2 (7).

A comparison of performance between the two different SBS cells - the capillary cell and the cell without the waveguide - reveals advantages and disadvantages for each.

Due to its longer interaction length, the capillary cell requires less peak-power input to reach SBS threshold than the non-capillary cell requires. This is proven by the fact that a long-pulse laser output could produce an SBS return in the capillary cell, whereas it could not in the other cell.

The capillary cell worked much better than the non-capillary cell with long-pulse laser output, but it operated very poorly with Q-switched laser output. If the Q-switched pulse caused any optical breakdown in the liquid, the resulting gas bubbles would be trapped in the capillary and completely block it. This was observed to happen several times; the gas bubbles would block the narrow capillary and prevent SBS from occurring on subsequent pulses. The non-capillary cell could operate better with Q-switched laser pulses, since the tiny gas bubbles could float to the top of the cell - out of the way of the next pulse.

Another difference between the two cells is their ease of alignment. The capillary cell required very precise alignment in order to get the maximum return from the cell. If the cell was slightly out of alignment, the laser beam would not remain confined within the capillary. The non-capillary cell had a much larger margin for error:

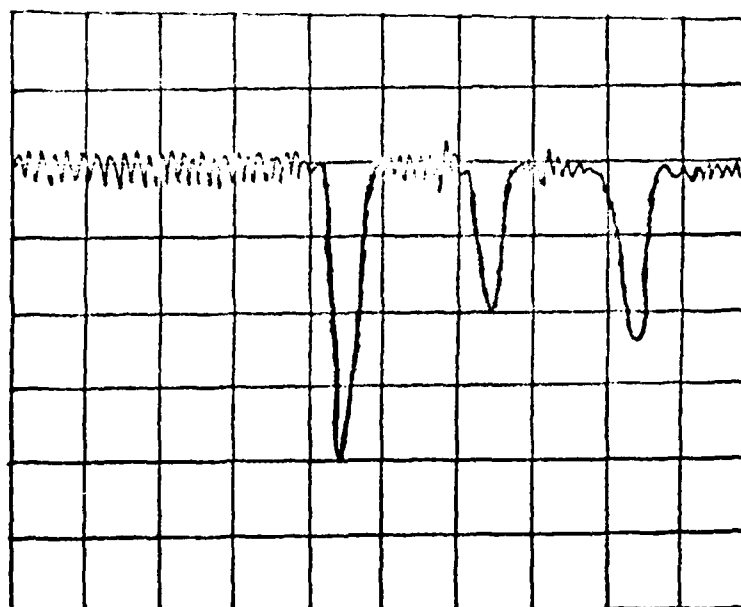


Figure 4.6 Temporal Shape of Long-Pulse
SBS Return (2 usec/div on horizontal axis)

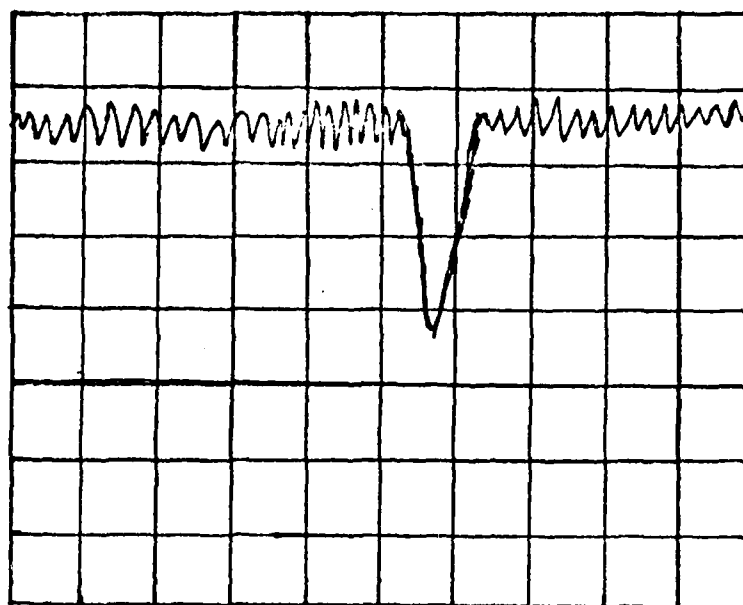


Figure 4.7 Q-Switched Temporal Characteristics
(20 nsec/div on horizontal axis)

could be moved several degrees off line and still work.

Aberrators Displaying Birefringence

The first category of aberrators discussed will be those displaying some form of birefringence. These include the Cornu Pseudodepolarizer and a sapphire quarter-wave plate. These aberrators affect the polarization of the incoming wave in some manner, depending on their construction and the polarization state of the incoming wave.

Cornu Pseudodepolarizer. The Cornu Pseudodepolarizer, made of optically active crystalline quartz, transforms linearly polarized light into a complex, spatially varying continuum of linear polarization states. Although not true depolarization, this complicated group of polarizations behaves very much like truly depolarized light. The amount of rotation of the incoming polarization is a continuous function of the y-coordinate on the face of the depolarizer, but is independent of the x-coordinate. The larger the beam diameter going into the CPD, the more rotation it undergoes. This means that a minimum beam diameter is required for complete depolarization. If this minimum diameter is not met, some residual polarization will remain in the beam. For more information on the operation of the CPD, refer to Reference (17:286).

Measurements with the polarization analyzer and the Laser Precision energy meter were made to determine the degree of depolarization achieved when the depolarizer was placed in the narrow beam (before the beam expander). The analyzer was placed after the depolarizer to determine how much energy was in the horizontal (p) polarization and how much was in the vertical (s) direction.

The sum of the energies passing through the analyzer at 0 degrees (p-polarized) and at 90 degrees (s-polarized) was 3.9 mJ. The measured energy passing through the analyzer at 90 degrees was 1.6 mJ; the energy passing through at 0 degrees was 2.3 mJ. The degree of polarization of the beam was

$$P = (P_p - P_s) / (P_p + P_s) \quad (18)$$
$$P = (2.33\text{mJ} - 1.56\text{mJ}) / 3.89\text{mJ}$$

$$P = .198$$

From eq (16), the depolarizer provides 80.2% depolarization when placed in the narrow part of the beam. Since the unpolarized portion of the beam consists, on the average, of 1/2 p and 1/2 s polarization, 0.59 of the beam is p-polarized and 0.41 of the beam is s-polarized.

The depolarizer changes the reflectivities of the beamsplitters, which changes the readings on the array and EG&G energy meters. To calculate the reflectivity with the depolarizer in place,

$$.59R_p + .41R_s = R_{\text{depol}} \quad (19)$$

$$(.59)(.008) + (.41)(.09) = R_{\text{depol}} = .041 \quad (20)$$

Eq (20) shows that the reflectivity of the beamsplitters has increased $(.041/.008) = 5.1$ times by placing the depolarizer in the beam. Energy readings taken on the EG&G meter must be corrected by this factor to compensate for this increased reflectivity.

According to Ref (9), if the light going into the SBS cell is depolarized, the SBS return will be diminished. This did not occur when the Cornu pseudodepolarizer was placed in the beam. The SBS return, measured on the EG&G meter, increased about 4 times in energy with the depolarizer present in the beam. On the contrary, after the 0.76 transmission of the depolarizer and the $(1/5.1)$ correction factor have been taken into account, the actual size of the SBS return stays about the same with or without the depolarizer. Apparently, enough residual polarization (19.8%) remains in the beam to prevent deterioration of the return.

In many cases, putting the depolarizer in the beam allowed enough energy to get to the diode array and the EG&G meter for good measurements. Without the depolarizer, the energy going to the array and meter was often too small to accurately detect. For this reason, the depolarizer was often used as a beam splitter reflectivity "enhancer".

Sapphire Quarter-Wave Plate. A birefringent sapphire quarter-wave plate was put into the beam at an angle so that the ordinary and extraordinary axes of the plate were at a 45 degree angle to the

horizontal polarization of the incident light. The plate was mounted just before the focusing lens in a manner which allowed it to slide various distances into the beam; Figure 4.8 illustrates this. In this way, the polarization of part of the beam could be changed, giving the beam two separate polarizations. The relative amounts of the two polarizations could be controlled by controlling the position of the plate.

As the plate moved further into the beam, the SBS energy measured on the EG&G meter increased. This increase is expected, since the reflectivity of the beamsplitters increases with the 90 degree rotation of polarization resulting from double-passing the quarter-wave plate. When the readings were corrected for this increase in reflectivity, the sapphire plate was found to have no effect on the reflectivity of the SBS cell; figure 4.9 shows this. These measurements were taken with cell A, but cell B gave similar results.

Aberrators which introduced birefringence into the beam had little or no effect on the SBS return. Using a sapphire plate to rotate part of the beam's polarization had no effect on the retro pulse, save to lower its intensity. After correcting for the transmission of the plate, the SBS reflectivity remained the same.

The Cornu Pseudodepolarizer appeared to have no effect on the SBS, either. According to Zel'Dovich, et al (30:148), high-fidelity phase conjugation requires either linearly or circularly polarized light. Since the CPD did not completely depolarize the beam apparently enough polarization remained in the beam to drive the SBS process.

The use of the CPD may have lowered the threshold for SBS to occur, but this was more of a "feel" than an observation. The increased reflectivity of the beam splitters could have made it appear on the array that SBS occurred only when the CPD was placed in the beam. A more sophisticated experiment is needed to decide if the CPD actually had any effect at all on the SBS reflectivity.

Aberrators Displaying Lensing Effects

The next category of aberrators discussed is aberrators having a

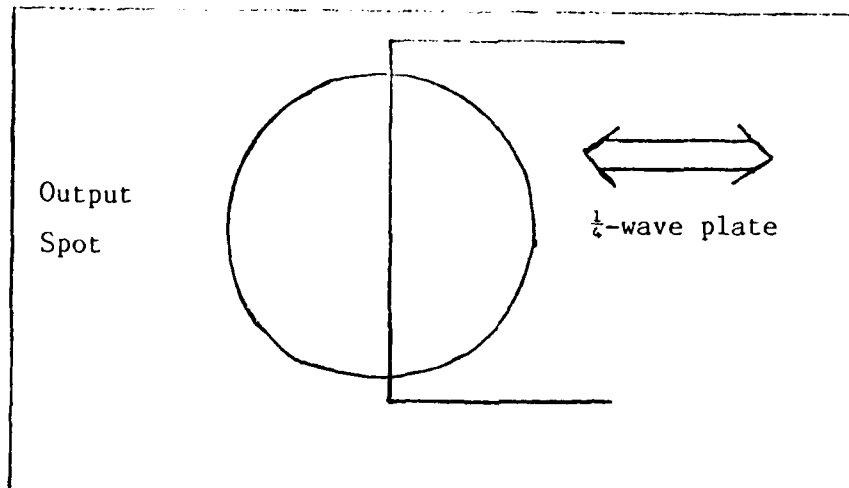


Figure 4.8 Sapphire Quarter-Wave Plate Sliding into Beam

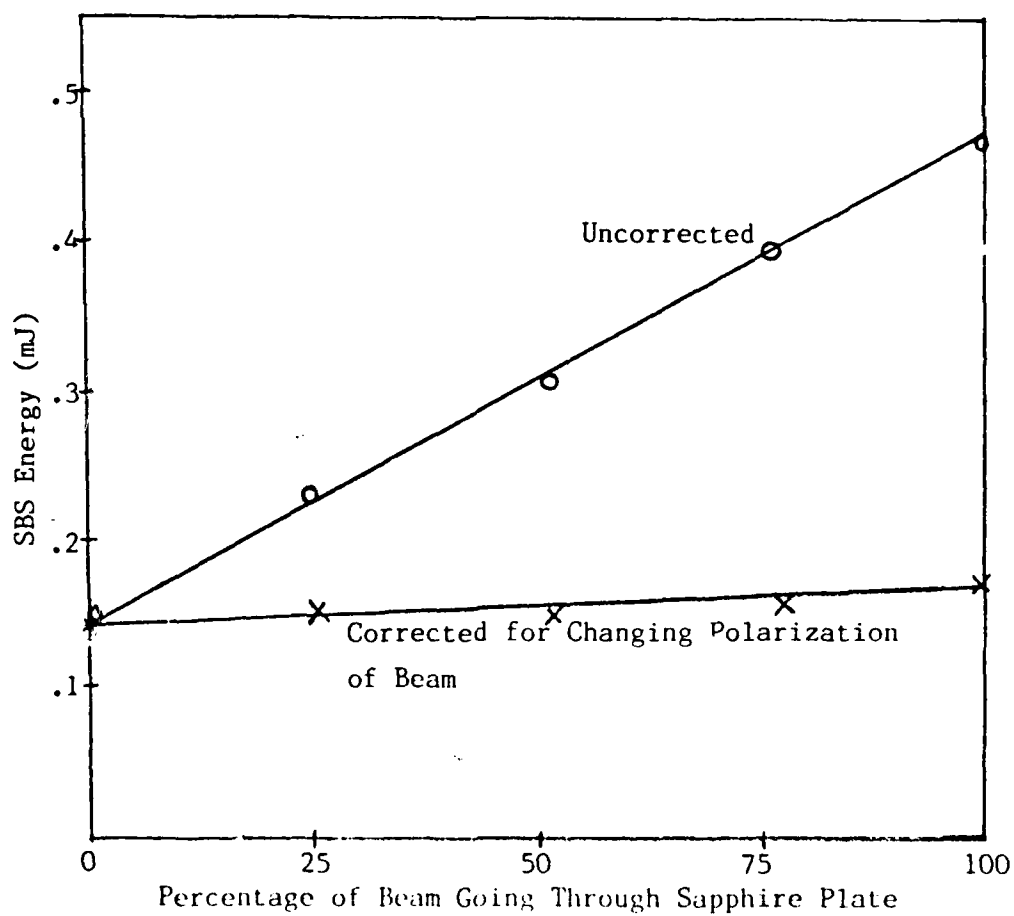


Figure 4.9 Energy vs. Sapphire Plate's Position in Beam

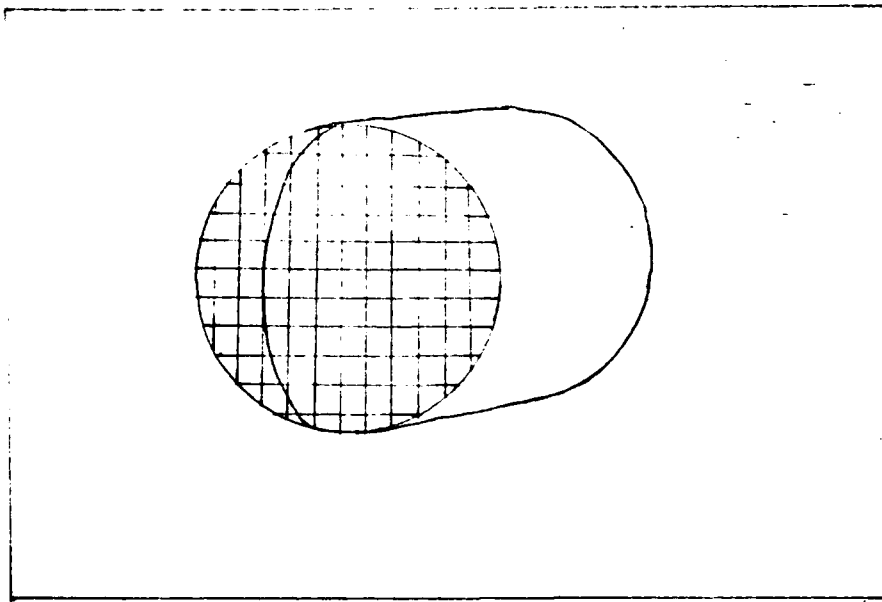


Figure 4.18 Large Screen

Large Screen. Energy measurements were taken for the large screen at the near field and far field points. Figure 4.19 gives the results of these measurements, taken using the capillary cell and long-pulse laser output. The points on the figure represent energy at the cell entrance (on the x-axis) and energy reflected back out of the cell (on the y-axis).

As figure 4.19 shows, the SBS return is again a linear function of the input energy to the cell. From the data in figure 4.19 and from equation (24), the SBS reflectivity of the cell is about 0.026. The cell reflectivity for the two dimensional aperture is about the same as for the 1-D case.

Figure 4.20 shows the return with the mirror in place of the cell and the focusing lens. Just as in the case of the one dimensional aperture, the mirror return is a linear function of input energy.

Figures 4.21a and 4.21b give the near-field spatial distribution of the SBS return and the mirror return, respectively. The two peaks in the left half of figure 4.21a are the SBS return. The peak in the right half of this picture is the spatial profile of the laser output pulse. Figure 4.21b shows only the return pulse with the mirror replacing the cell and focusing lens. The SBS return has significantly

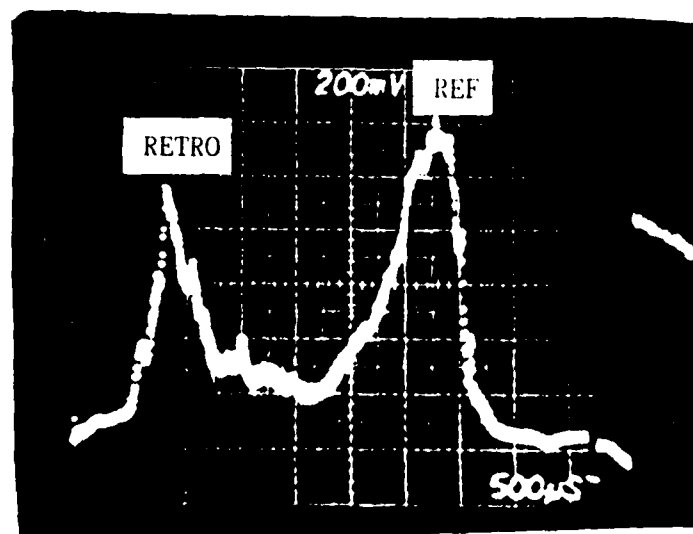
placed in the far field. Figure 4.16a and figure 4.16b show the SBS return and the mirror return, respectively. Comparison of these two pictures with the ones in figure 4.15 shows that the spatial profile of the SBS pulse stays about the same in near or far field. Unlike the SBS profile, the spatial profile for the mirror return deteriorates noticeably when the aperture stack is moved from the near field position to the far field position.

These energy and spatial profile measurements were made using the capillary SBS cell. One problem with this cell that became evident is that part of the diffraction pattern from the apertures (visible with the HeNe laser) misses the capillary entrance. Only the central spot from the diffraction pattern enters the capillary; the rest of the pattern is lost. This means that the SBS cell cannot reflect all of the energy that reaches it, nor can it completely correct for the presence of the apertures. This problem might have been corrected by using the SBS cell without the capillary waveguide; unfortunately, the SBS threshold for this cell was too high to produce a return with the seven aperture stack.

Q-switched measurements were not taken with this aberrator, due to the erratic results obtained. The Q-switched laser output would create bubbles from plasma breakdown in the capillary; these bubbles were large enough to completely block the capillary and stop the SBS process.

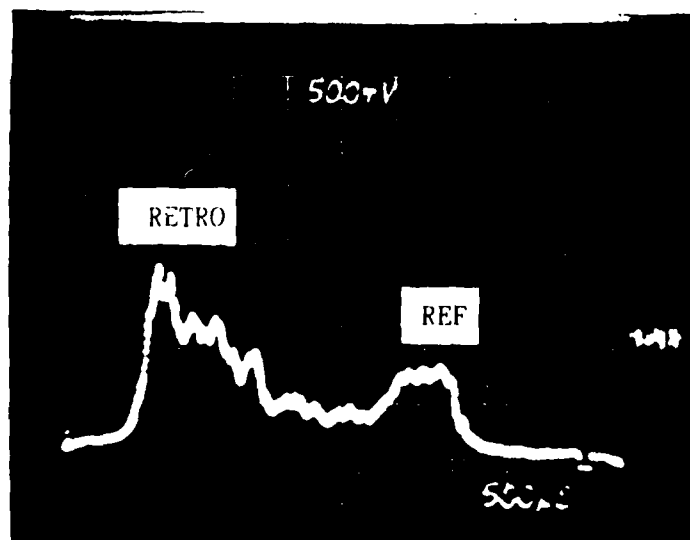
Two Dimensional Apertures

A natural step from one dimensional apertures is to two dimensional apertures. Rather than using overlapping slides to form the apertures, wire-mesh screens were used. These pieces of screen resembled ordinary window screen. Two different sizes of wire mesh were used: the larger mesh had a 1.8 mm spacing between wires, the finer mesh had a 0.3 mm spacing. Figure 4.18 shows a sketch of the large screen. The transmission of the large screen was measured with the Laser Precision meter to be 0.65 . The fine screen had a transmission of 0.28.



a

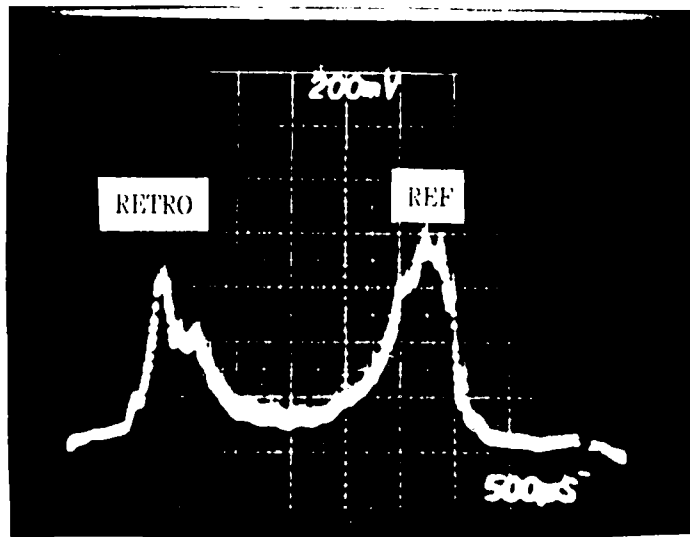
.1 inch/div



b

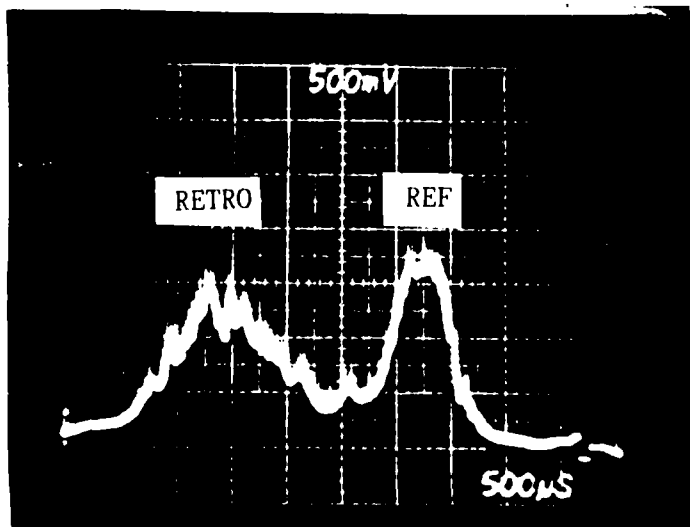
.1 inch/div

Figure 4.16 Spatial Distribution of Return Pulse with
7 Aperture Stack in Far Field a) SBS b) mirror



a

.1 inch/div



b

.1 inch/div

Figure 4.15 Spatial Distribution of Return Pulse with 7 Aperture Stack in Near Field a) SBS b)mirror

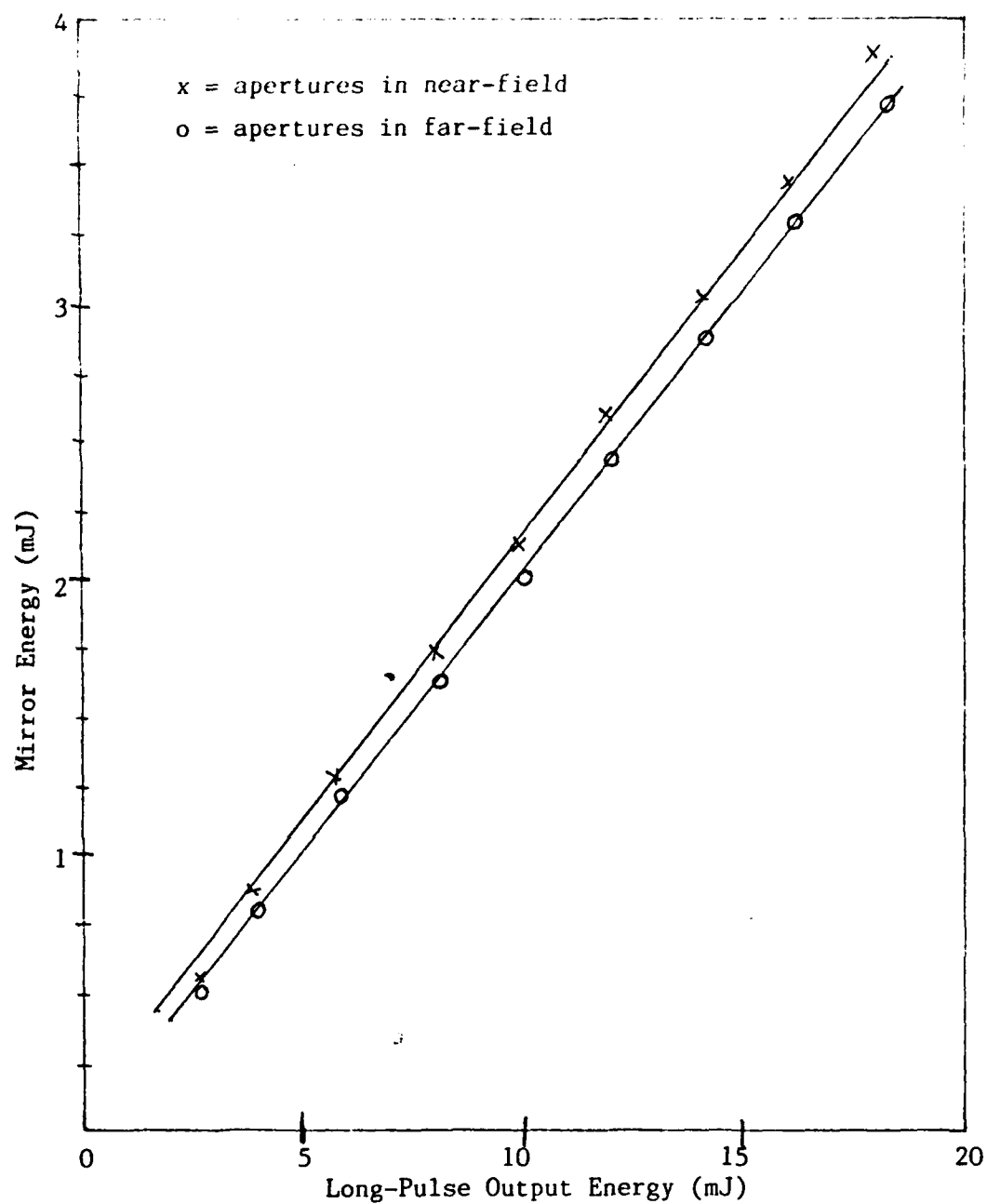


Figure 4.14 Mirror Return Energy vs Output Energy -
7 Aperture Stack

The reflectivity of the SBS cell can be calculated from these energy measurements. For a laser output of E_0 (measured after the beam splitters with the Laser Precision meter), the energy reaching the cell is

$$E_{\text{cell}} = E_0(.95)(T_{\text{aberrator}})(T_{\text{lens}}) \quad (22)$$

$$E_{\text{cell}} = (.95)(.479)(.918)E_0 = .418E_0$$

The SBS energy reflected from the cell, after correcting the meter reading, is

$$E_{\text{sbs}} = E_{\text{meter}} / [(.95)(T_{\text{aberrator}})(T_{\text{lens}})] \quad (23)$$

$$E_{\text{sbs}} = E_{\text{meter}}(2.394)$$

Dividing equation (23) by equation (22) gives the reflectivity of the cell. Inserting a calibration factor of 0.37 to convert the EG&G meter reading to mJ,

$$R_{\text{SBS}} = .487E_{\text{meter}}/E_0(T_{\text{aberrator}})^2 \quad (24)$$

From equation 24, the cell reflectivity in the presence of the seven aperture stack is 0.026 .

A second set of energy measurements was taken with a $R=.99$ flat mirror replacing the SBS cell and lens. These measurements appear in figure 4.14. The data is linear for near and far field, just as the SBS return energy data was.

Figure 4.15 shows the spatial distribution of the pulse in the near field. The peak on the right of the photograph is the laser output pulse; the peak on the left is the retro pulse. Figure 4.15a shows the SBS retro, while figure 4.15b shows the retro pulse with the mirror replacing the SBS cell and lens. The peak for the SBS return is sharper and better defined than the peak for the mirror return. This shows that the divergence for the SBS return is smaller than for the mirror return - SBS is correcting for the divergence introduced by the apertures.

Figure 4.16 shows the spatial profile for the seven aperture stack

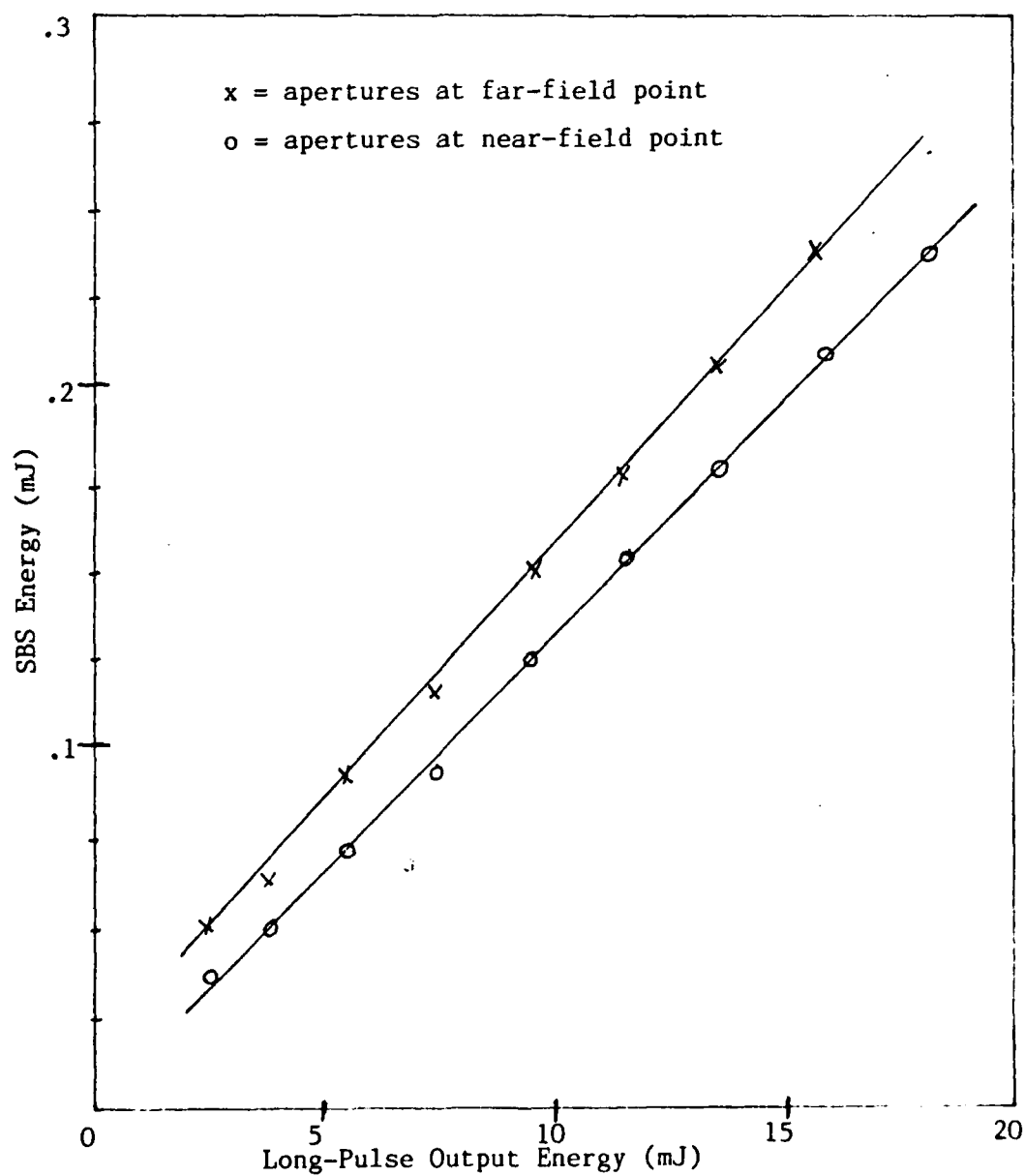


Figure 4.13 SBS Energy vs Output Energy - 7 Aperture Stack

the far field (point 2 in figure 3.1). Figure 4.13 shows the SBS energy vs long pulse laser output.

The SBS energy vs laser output energy has a fairly linear relationship. Figure 4.13 shows that the near field return is consistently less than the far field return. This may be explained by the presence of dirt and smudges on the slides. The beam was hitting one of the smudges when the stack was in the near field, which cut down the transmission. When the stack was moved slightly, the SBS return increased to a level slightly above that of the far field position.

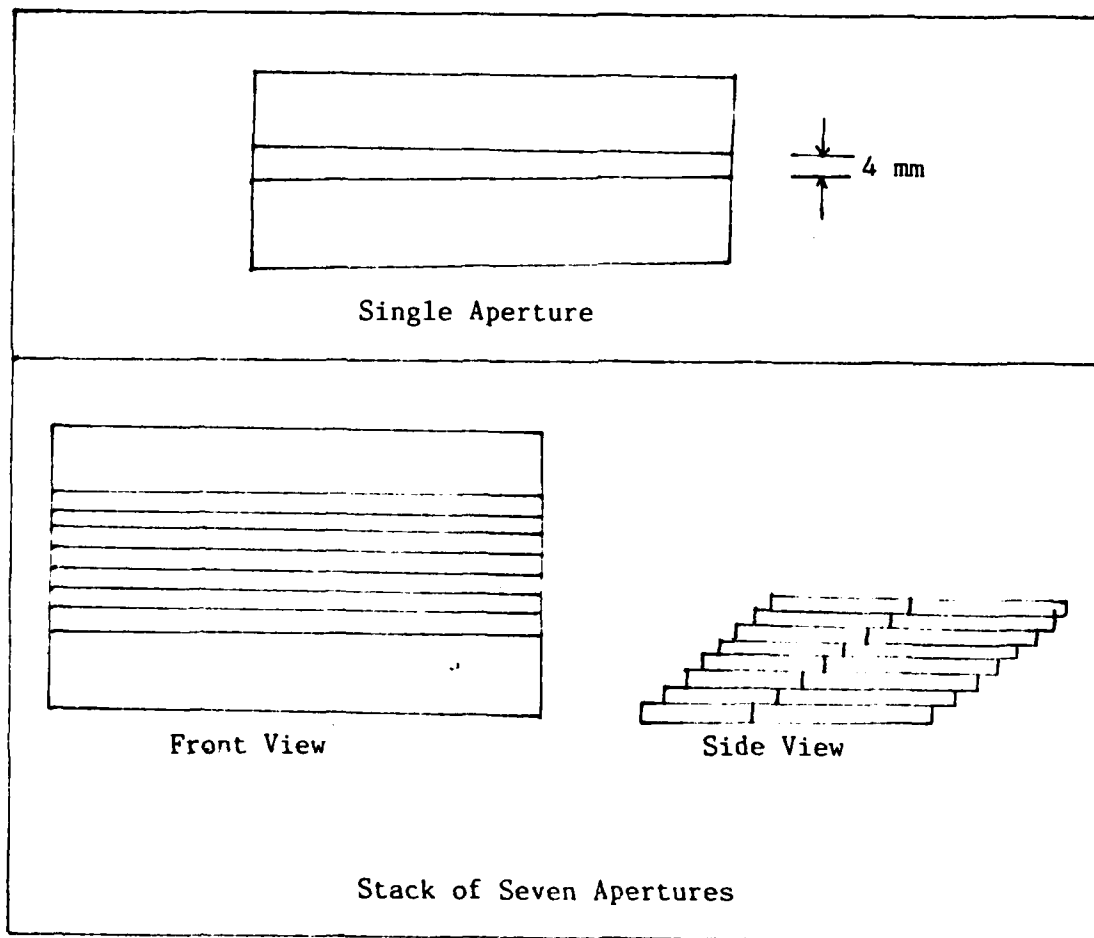


Figure 4.12 Construction of One-Dimensional Apertures from Overlapping Microscope Slides

The 250 mm lens effectively shortens the focal length of the 1m focusing lens in one dimension, leaving the other dimension unchanged. The combination of the focusing lens and the cylindrical lens may be viewed as a single lens with different focal lengths in the x- and y-dimensions. If the SBS return could correct for the phase front curvature introduced by the focusing lens, then it should also be able to correct for the phase curvature introduced by this asymmetric lens combination.

The collected data confirmed the above hypothesis: the SBS reflection could, indeed, correct for the distortions introduced by an asymmetrically-focusing lens or combination of lenses.

One Dimensional Apertures

The next type of aberrator investigated is the one dimensional aperture. Both a single aperture and a multiple stack of apertures were investigated. These apertures were constructed by overlapping various numbers of microscope slides. The single aperture consisted of two slides overlapping by 4mm, as shown in figure 4.12.

Figure 4.12 also shows the construction of the multi-aperture stack. This stack consists of 16 slides overlapping to create 7 apertures. The stack of apertures was created by overlapping 8 of the single aperture units shown in figure 4.12. The stack was made in this way so that the entire beam would go through the same thickness of glass. If one part of the beam went through a different number of slides than another part, the amount of energy reflected by the slides would differ for different parts of the beam. Keeping the thickness of the stack uniform over all seven apertures made the beam aberration a function of the apertures only. The transmission of the seven aperture stack, measured on the Laser Precision meter, is 0.48.

Measurements were first taken with the single aperture shown in figure 4.12. The single aperture did very little to aberrate the beam, thus proving to be an uninteresting case for study.

The seven aperture stack aberrated the beam greatly, as evident in the He Ne laser's visible diffraction pattern. Measurements were taken both with the stack in the near field (point 3 in figure 3.1) and in

The cylindrical lens did not significantly improve either the magnitude or the consistency of the SRS return, as the above numbers show.

The fact that the SRS return did not change very much when the cylindrical lens was in place shows that SRS can compensate for an aberrator which acts like a cylindrical lens. Since the 250 mm lens has a short focal length, it would cause the beam to diverge greatly on the way back to the energy meter and diode array. If the lens was not compensated for, the beam diameter would have been quite large by the time it traversed the distance to the energy meter and the diode array. The fact that the energy reading did not greatly decrease when the cylindrical lens was put into the beam shows that the beam diameter did not increase greatly, and that the SRS return must have compensated for the effects of the lens. This was confirmed by observing the beam's spatial distribution on the diode array. The width of the spatial distribution remained about the same when the lens was placed in the beam.

The aberrators tested which have focusing effects on the beam did not degrade the SRS return. The cylindrical lens telescope, which reduced the beam diameter in one dimension, had no effect on the SRS return. This result is not too surprising, since the beam should have returned to its original dimensions after going back through the telescope, with or without SRS. An energy loss occurred in the SRS cell because the telescope caused the beam to focus to a larger diameter spot, which would not completely fit into the capillary. Other than this energy loss, the cylindrical lens telescope had no other effect on the SRS return.

The single 250 mm cylindrical lens also had no effect on the SRS return. After correcting for the transmission of the lens, the reflectivity of the cell remained the same with or without the lens in place. The spatial distribution of the return was also unaffected by the lens. This result is also to be expected, since the SRS return must correct for the divergence introduced by the 1m focusing lens in order to work without any aberrators present. The focusing lens causes a curvature of the phase fronts, which the SRS return corrects for upon passing back through the lens.

4.11 shows, not all of the energy will go down the waveguide. If part of the energy is lost outside the waveguide, this would certainly diminish the energy in the return pulse. The situation shown in Figure 4.11 was, in fact, observed with the HeNe alignment laser and is probably the reason for the decreased energy returns.

Repeating the experiment with Q-switched output, with and without the depolarizer in place, gave similar results. Consistent SBS could not be achieved with cell A, so only cell B - the capillary cell - was used for this section of the experiment.

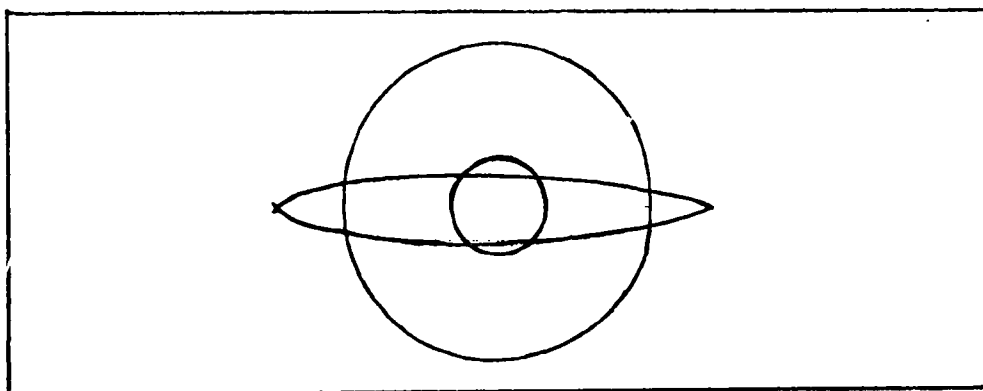


Figure 4.11 Focal Spot from Cylindrical Telescope

Single Cylindrical Lens. A single 250 mm cylindrical lens was mounted right next to the cell entrance. This caused the x-dimension of the beam to focus at a slightly different spot in the cell than the y-dimension of the beam, thereby lowering the peak power density.

The data, taken with the laser Q-switched, is

w/o lens:	average E_{SBS} = 0.01 mJ
	σ = 0.51 mJ
w/ lens:	average E_{SBS} = 0.01 mJ
	σ = 0.85 mJ

where

s = focal spot size

λ = wavelength

f = focal length of lens

d = diameter of incoming beam (27:75)

Equation (21) shows that as the diameter of the incoming beam decreases, the focal spot size increases. This could affect the SBS return in several ways.

Table I
Transmissions of Various Focal-Length Cylindrical Lenses

Focal Length (cm)	Transmission
-67	0.95
40	0.92
45	0.68
62	0.95
100	0.96
250	0.94

The most obvious effect that this increased focal spot could have is to lower the peak power density inside the cell. This could reduce the magnitude of the SBS return, reduce the amount of plasma breakdown occurring, or both; neither of these was observed, however.

Another way that the increased focal spot size could affect the SBS is to cause part of the beam to miss the SBS cell. When the cylindrical lens telescope decreases the beam diameter, the focal spot may become bigger than the capillary diameter in the cell. As figure

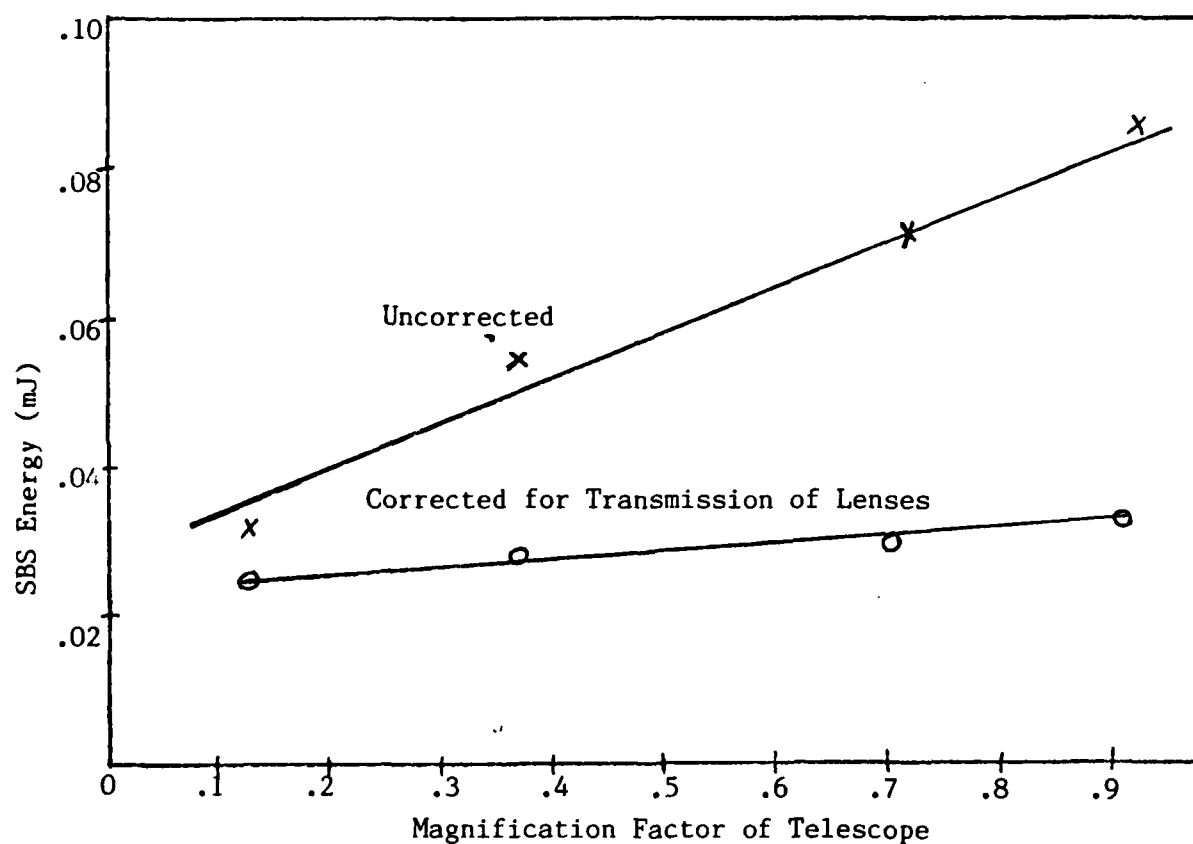


Figure 4.10 SBS Return vs Magnification of Cylindrical Lens Telescope

lensing or focusing effect on the beam. Changing the focusing of the beam changes the focal spot size, and therefore changes the peak power density inside the cell.

Cylindrical Lens Telescope. To change the focusing of the beam, a cylindrical lens telescope was placed in the beam just in front of the focusing lens. The telescope, consisting of two cylindrical lenses, was constructed so that the diameter of the beam decreased in the y-direction, while the diameter in the x-direction remained unchanged. The lenses were placed a distance from each other equal to the sum of their focal lengths, so the beam remained collimated after passing through the telescope. Various combinations of focal lengths gave different "powers" of expansion. For example, a 100 mm cylindrical lens and a 25 mm cylindrical lens would provide an expansion of $(25/100) = 0.25$. This means that the beam's diameter would be only 1/4 as large as before in the y-direction, while remaining unchanged in the x-direction.

Each of the five cylindrical lenses used in this experiment had a different transmission factor. To determine this factor, a single lens was put in the beam path and the energy throughput of the lens was measured using the Laser Precision energy meter. Table I gives the transmission factors for the various lenses used.

Energy readings of the SBS return with different combinations of lenses in place were taken on the EG&G meter. The laser output was long-pulse, and the depolarizer was used to obtain higher reflectivity from the beam splitters (this allowed better readings on the meter). Figure 4.10 gives the SBS energy (after correcting for the transmission factors of the lenses) vs the expansion factor of the telescope. As figure 4.10 shows, the SBS energy increases as the expansion factor of the telescope increases toward 1. This means that the energy decreases as the beam gets more "compacted". This result arises from a property of the focusing lens.

The focal spot size of a diffraction-limited circular lens is given by

$$s = 1.22 \lambda f/d \quad (21)$$

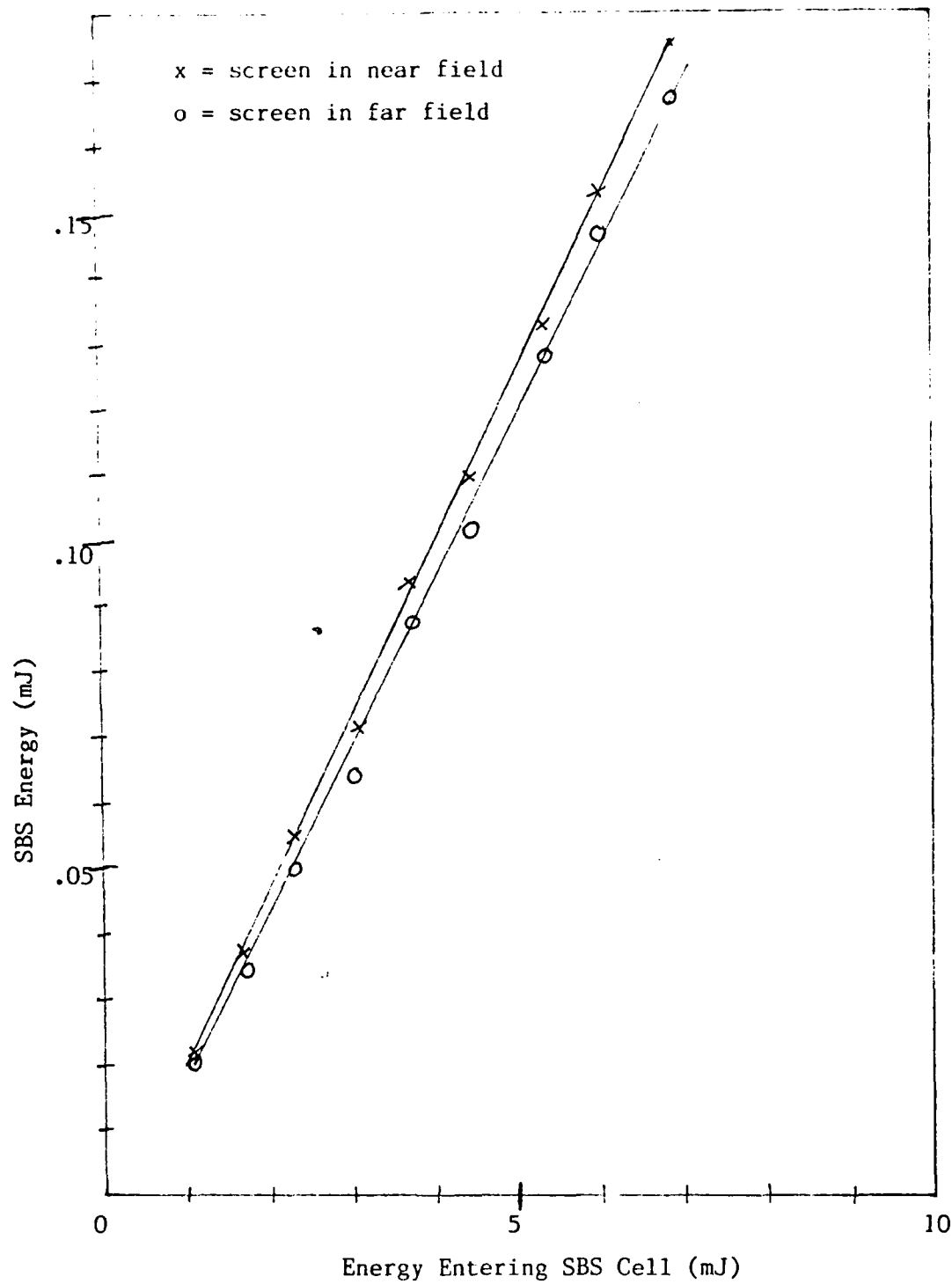


Figure 4.19 SBS Energy vs Input Energy - Large Screen

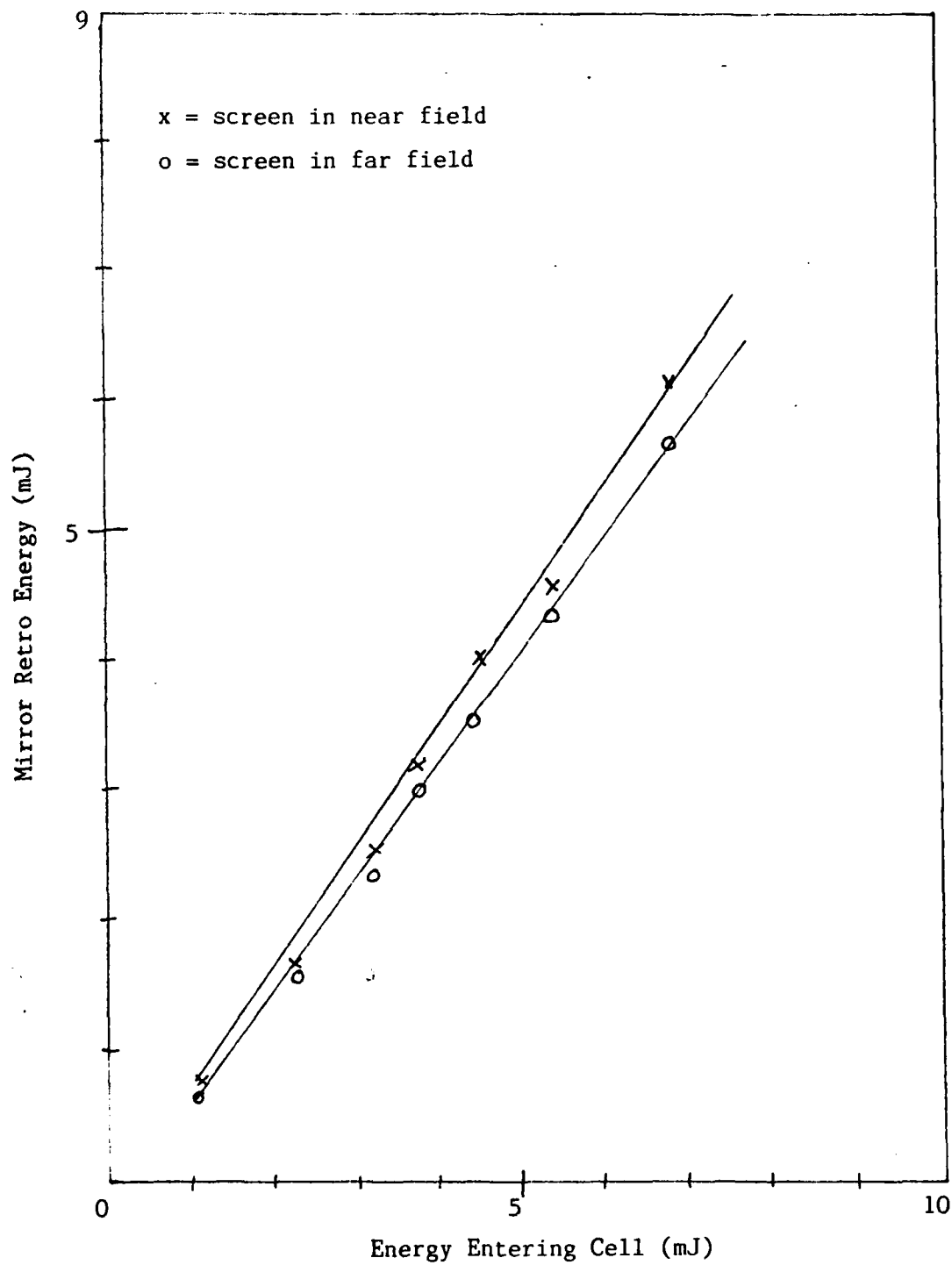


Figure 4.20 Mirror Retro Energy vs Input Energy - Large Screen

less spatial modulation than the mirror retro pulse. The many peaks in the mirror retro spatial distribution result from the diffraction due to the large screen.

Figures 4.22a and 4.22b give the spatial distributions of the SBS return and the mirror return with the large screen in the far field. The format of these photographs is the same as those in figure 4.21. The SBS corrects for some of the spatial modulation introduced by the screen, but not as well as in figure 4.21a. Much of the modulation remains in the spatial profile, though there is some reduction from the amount of modulation present in the mirror return (figure 4.22b).

As with the one dimensional apertures, the 2-D apertures' diffraction pattern was too large to get into the capillary. Only the central spot of the pattern went down the capillary waveguide; the rest of the energy in the pattern was lost. This helps explain the low reflectivity of the cell and the incomplete correction for the apertures.

Fine Screen. Measurements were attempted with the fine screen in the near field, but readings could only be taken with the laser at maximum long pulse output energy. The low transmission of the screen, along with much of the diffraction pattern missing the capillary entrance caused a very low energy return. The SBS energy, with the fine screen at the near-field point and with 3.0 mJ entering the cell, is

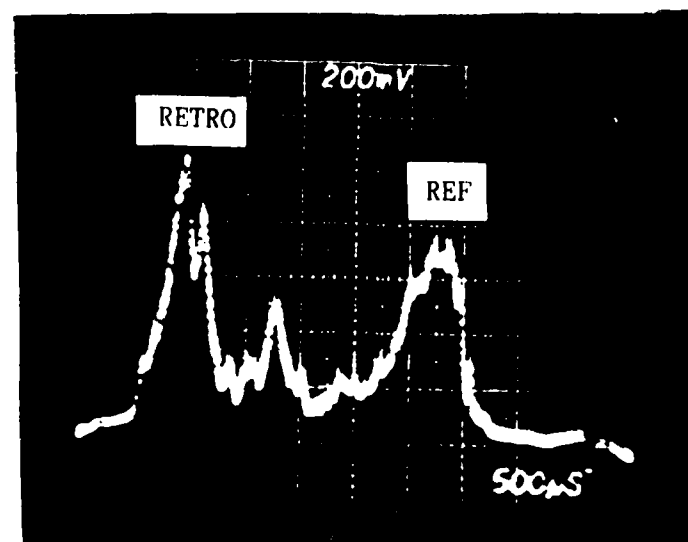
$$E_{\text{SBS}} = 0.06 \text{ mJ}$$

This energy value gives a reflectivity of $R_{\text{SBS}} = 0.02$, which is fairly close to the reflectivity value of 0.026 for the large screen.

The energy of the SBS return with the fine screen in the far field is

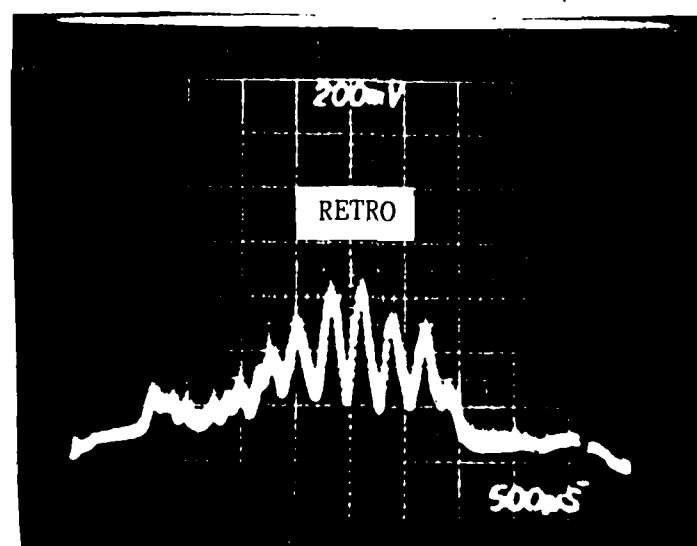
$$E_{\text{SBS}} = .05 \text{ mJ}$$

giving a reflectivity of $R_{\text{SBS}} = 0.017$. This measurement was also taken with the laser at maximum output power. The energy with the fine screen in place was too low to obtain a good picture of the spatial



a

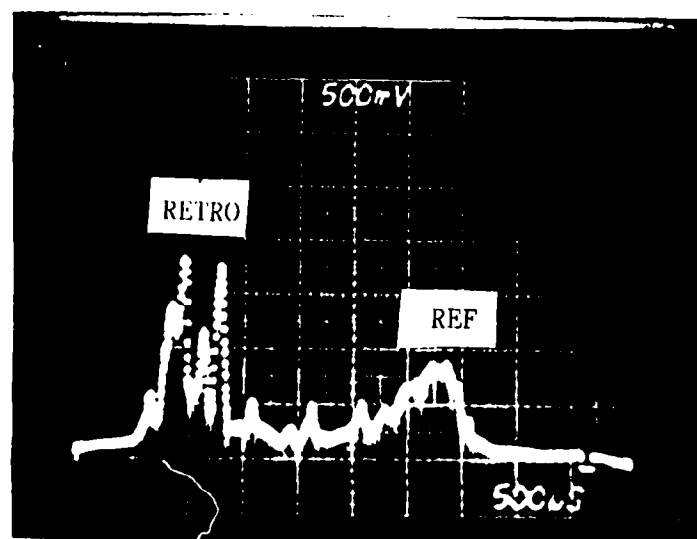
.1 inch/div



b

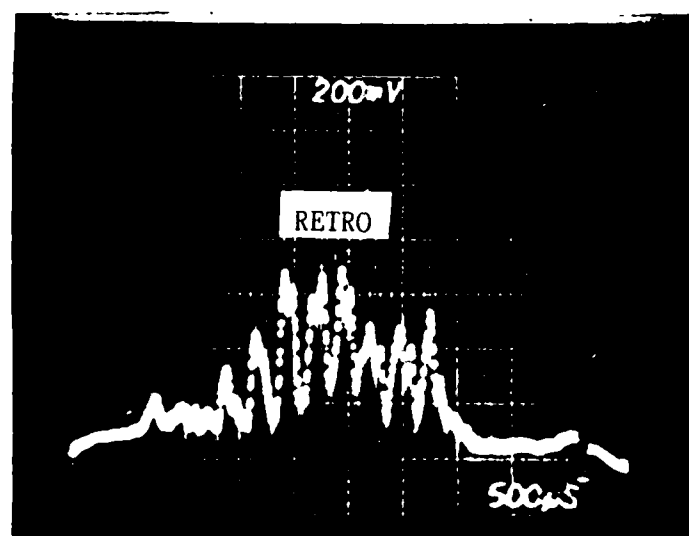
.1 inch/div

Figure 4.21 Spatial Distribution of Return Pulse with Large Screen in Near Field; a) SBS b) Mirror



a

.1 inch/div



b

.1 inch/div

Figure 4.22 Spatial Distribution of Return Pulse with Large Screen in Far Field; a) SBS b) Mirror

profile on the diode array.

The measurements of energy and spatial profile for both the large and the fine screens were taken using the capillary cell. The lower SBS threshold of this cell, along with long pulse laser output, were necessary to get any degree of consistency in the measurements. The experiment with the large screen was done with the other SBS cell, but Q-switched output was needed to reach SBS threshold. The use of Q-switched output resulted in highly inconsistent data, making the results very difficult to interpret.

Miscellaneous Aberrators: 50% Beam Splitter

The final aberrator to be discussed is a 50% beamsplitter. This device, shown in figure 4.23, is a piece of glass coated with a reflective layer. This reflective coating has regularly spaced holes in it which allow 50% of the light through. Due to these holes in the coating, the 50% beam splitter also acts as a two dimensional diffracting element.

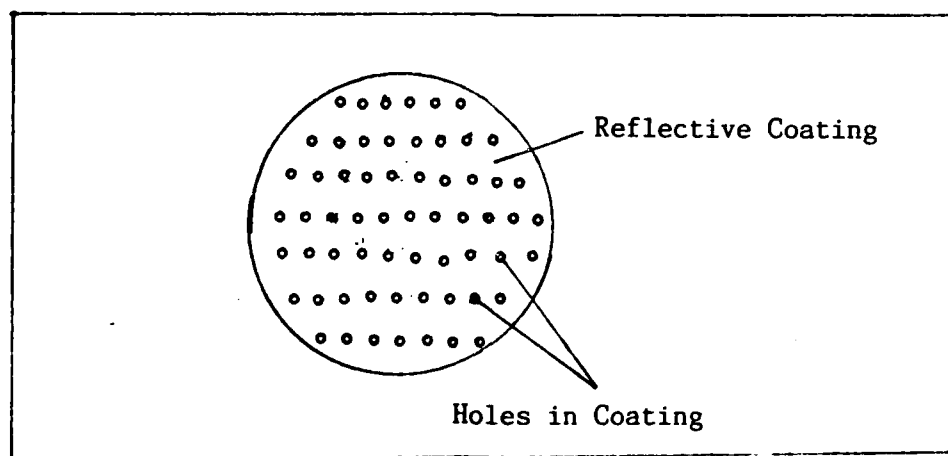


Figure 4.23 50% Beam Splitter

Energy measurements, taken with the capillary cell and long pulse laser output, appear in figure 4.24. Once again, the SBS energy is a linear function of the input energy. Figure 4.25 gives the retro pulse energy with the mirror replacing the SBS cell and lens. From equation (24) and the data in figure 4.24, the SBS reflectivity is

$$R_{\text{SBS}} = 0.023$$

which is very close to the reflectivity with the large screen in place.

Figures 4.26 and 4.27 show the spatial profiles with the beam splitter in the near and the far field, respectively. Comparing figure 4.26a (SBS return in the left half of the picture, laser output pulse on the right) with figure 4.26b (retro pulse with mirror in place of the cell and lens) shows that the SBS pulse diverges less than the mirror pulse. This means that the SBS compensates to some degree for the aberrations introduced by the beam splitter. This same compensation was evident when the beam splitter was placed at the far field point, shown in figure 4.27.

The problem with the the diffraction pattern missing the capillary occurred for the 50% beam splitter, just as it did for the other diffraction elements. The diffraction pattern resembled that of the large screen.

Though by no means completely conclusive, the data on one-dimensional and two-dimensional apertures indicates some degree of correction for distortions introduced by the apertures. The spatial distribution of the SBS return had less diffraction-induced spatial modulation than the return with the normal mirror had; the central peak of the SBS retro pulse was more defined than the central peak of the mirror return.

Since the capillary cell was used for the aperture experiments, not all of the diffraction pattern fit into the capillary entrance. This energy loss meant that the SBS return could not possibly correct completely for the distortions in the beam due to the apertures. Since part of the energy was lost, part of the "information" needed by the SBS cell to correct for the diffraction caused by the apertures was

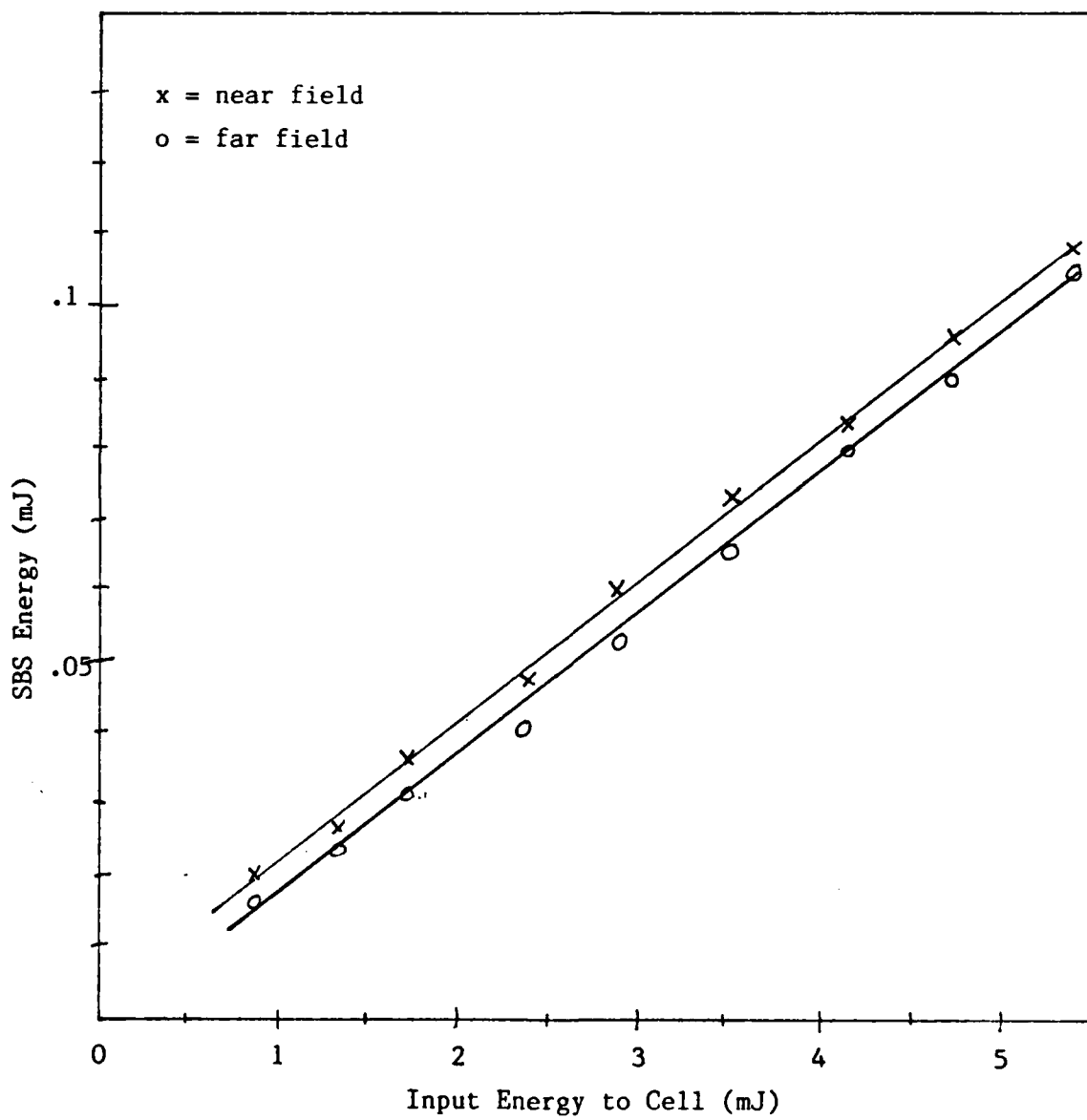


Figure 4.24 SBS Energy vs Input Energy - 50% Beam Splitter

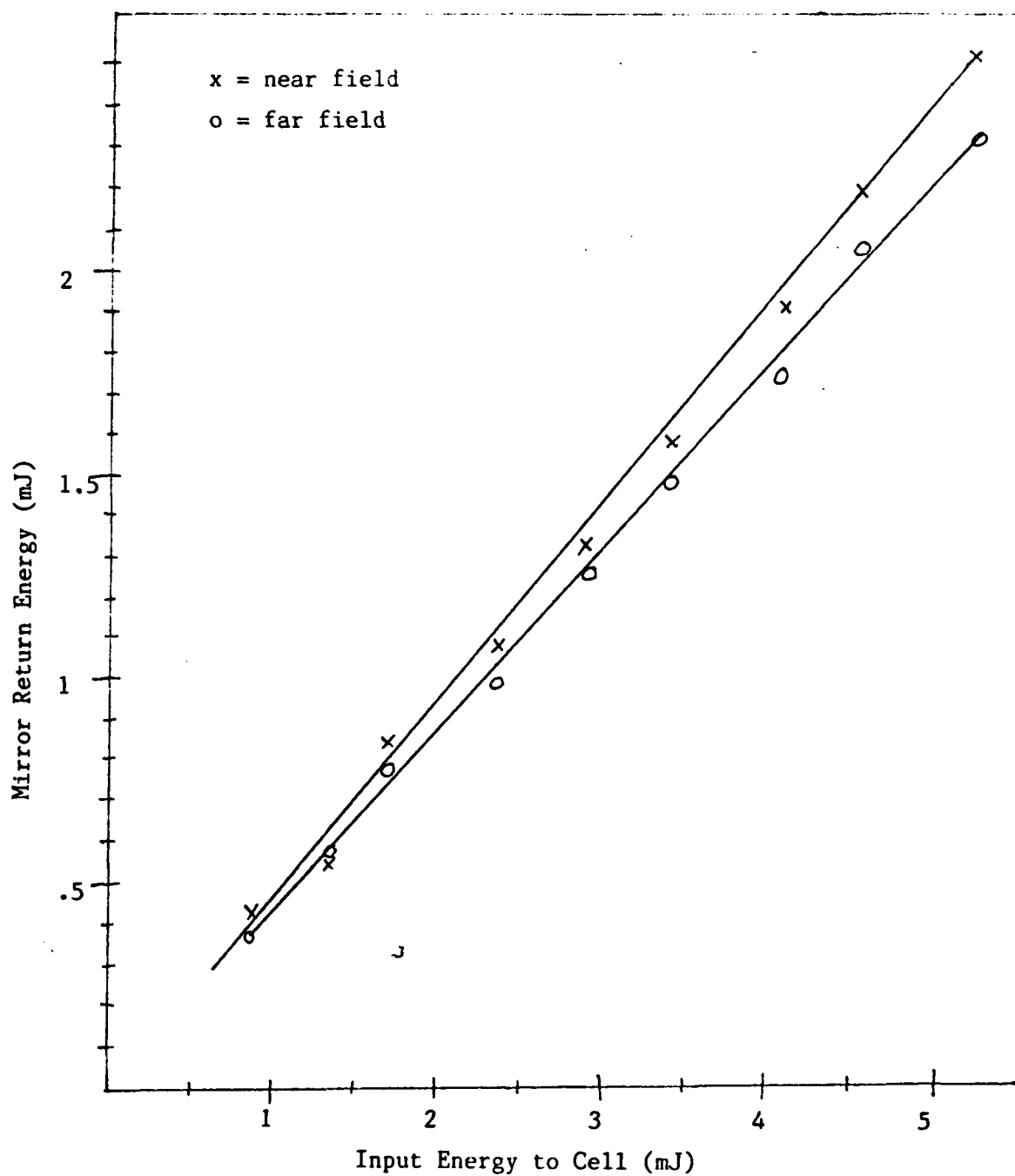
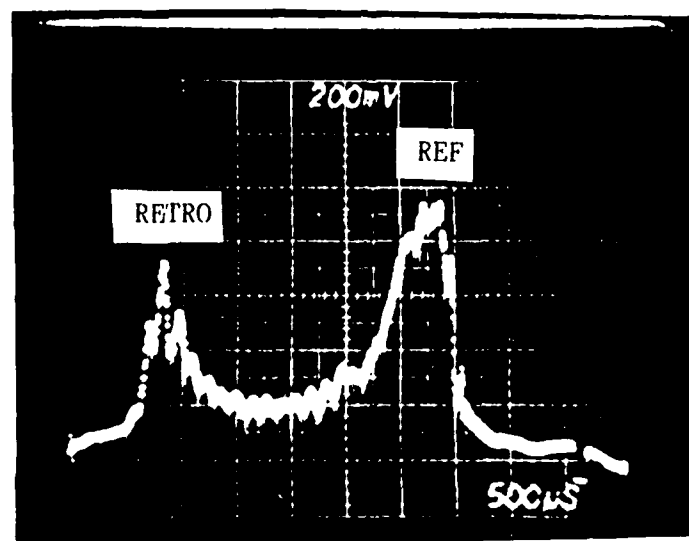
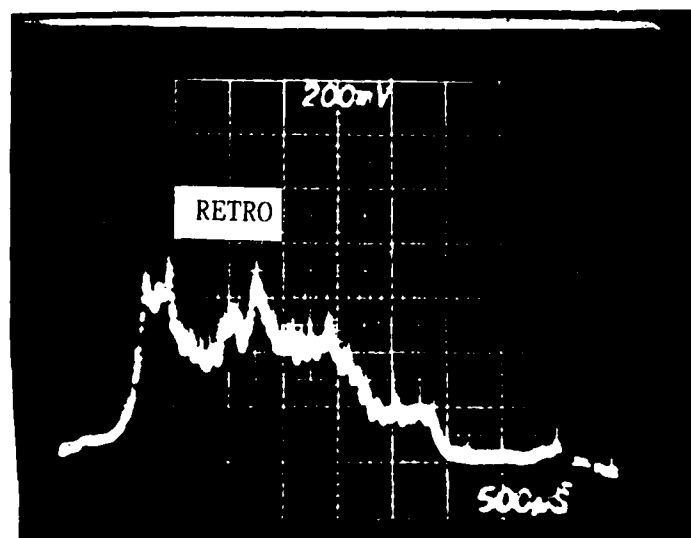


Figure 4.25 Mirror Return Energy vs Input Energy -
50% Beam Splitter



a

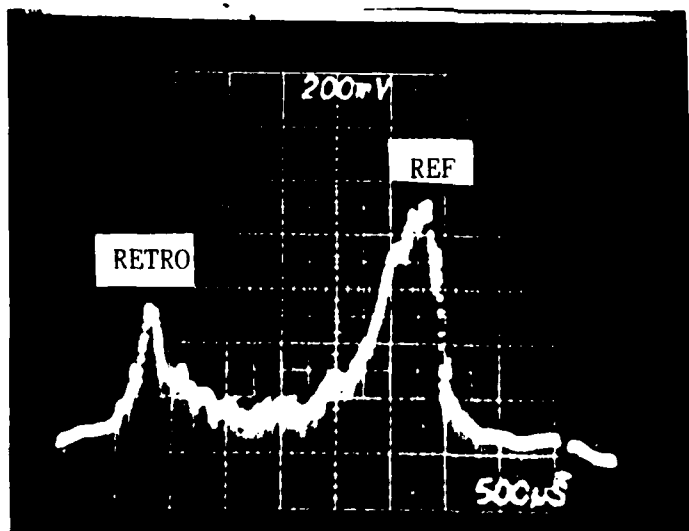
.1 inch/div



b

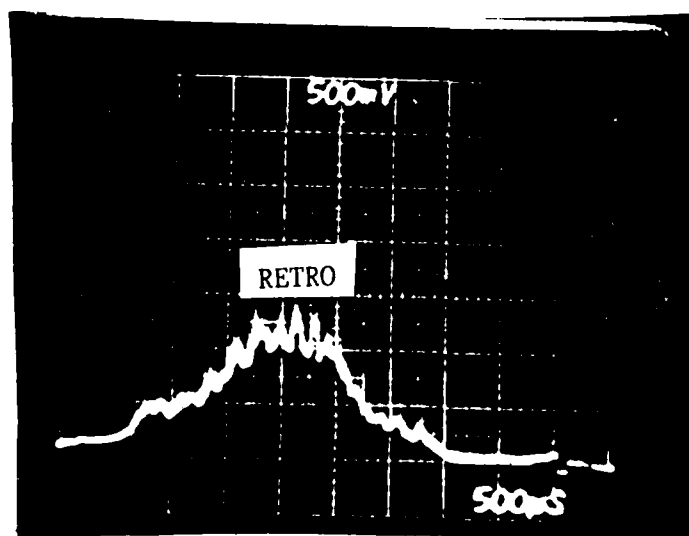
.1 inch/div

Figure 4.26 Spatial Distribution of Return Pulse with 50% Beam Splitter in Near Field;; a) SBS b) Mirror



a

.1 inch/div



b

.1 inch/div

Figure 4.27 Spatial Distribution of Return Pulse with 50% Beam Splitter in Far Field; a) SBS b) Mirror

lost. Without complete "information", the SBS process can only partially correct for the distortion of the beam.

Even if a non-capillary cell with a high SBS reflectivity were used, part of the diffraction pattern focused into the cell would undoubtedly be of insufficient intensity to reach SBS threshold. The information in part of the diffraction pattern would again be lost, since only part of the diffraction pattern would be retro-reflected.

In order to get complete correction, all of the diffraction pattern must be reflected by the SBS cell. Since the spatial distribution of the diffraction pattern extends over an infinite area, this could actually never occur. By capturing the first few cycles of the diffraction pattern in the SBS cell, a very high percentage of the pattern's energy could be reflected. This would provide a near-complete degree of correction, assuming that all of the pattern entering the cell exceeded SBS threshold. A way to achieve this will be suggested in the last section of this thesis.

V. Problems, Conclusions, and Recommendations for Further Study

This chapter discusses problems encountered during the experiment, conclusions drawn from the data presented in the previous chapter, and recommendations for further study. The problems encountered during the experiment often had an impact on the data taken, therefore these problems merit discussion. The conclusions drawn from the presented data include the degree of compensation provided by the SBS reflection for aberrations, as well as any trends which became apparent in the data. The recommendations for further study stem from questions unanswered by this experiment.

Problems Encountered During Experimentation

Several problems, both minor and major, affected the results of the experiment. These ranged from matters such as lack of a proper clamp to hold a component, to things such as the inability of the energy meters to accurately detect the retro pulse energy.

Energy Meters. In order to be sensitive enough to detect the small energy levels present in the retro pulses, the meters had to operate without narrow beam adapters and on their most sensitive scale. Operation with no narrow beam adapter meant that the energy registering on the meter depended on the location of the spot on the detector surface. The use of the most sensitive scale made the meters inherently unstable and difficult to balance. Both of these factors contributed variations to the collected data.

Laser. The laser used in this experiment had an inconsistent output in terms of energy/pulse and spatial distribution, which created unwanted variation in the input energy to the cell.

Beam Splitters. The interference from the front and back surface reflections of the flat, uncoated beam splitters created variations in the spatial distributions of the pulses on the diode array. This interference from the beam splitters made it difficult to determine the degree of spatial correction for aberrations provided by SBS. Wedged

or AR-coated beam splitters would have helped this problem by eliminating the interference originating from the beam splitters.

Mounting Hardware. Often during the experiment, equipment had to be mounted with unstable or ill-fitting clamps. These clamps had no fine adjustments and would often slip out of alignment in the middle of an experiment.

Interferometer. Perhaps the greatest problem during the experiment arose from the use of an interferometer to measure the percentage of the backscattered pulse which is phase-conjugated (9). This interferometer appears in figure 5.1. The beam splitter creates

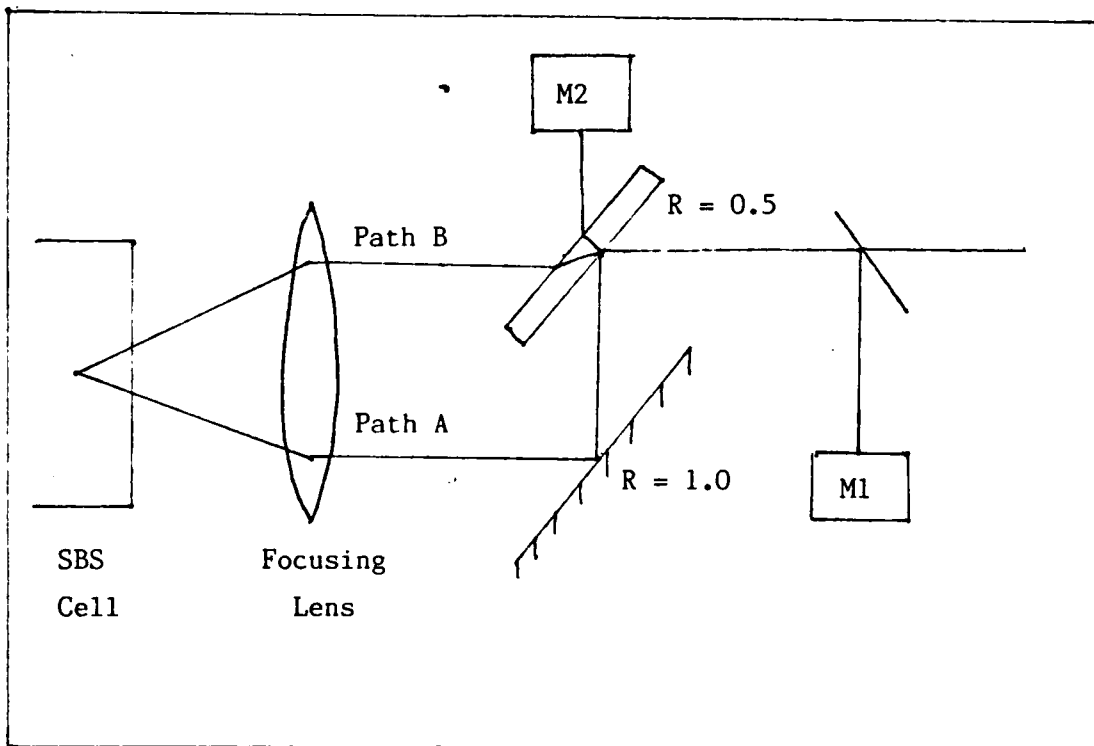


Figure 5.1 Interferometer Used to Measure Phase Conjugation Quality

$$y = (E_A + E_B \cos z) \sin wt - (E_A + E_B \sin z) \cos wt \quad (31)$$

Let

$$E_A + E_B \cos z + A \cos \theta \quad (32)$$

$$E_B \sin z = A \sin \theta \quad (33)$$

Therefore,

$$\tan \theta + E_B \sin z / (E_A + E_B \cos z)$$

Squaring and adding equations (32) and (33),

$$\begin{aligned} E_A^2 + E_B^2 (\cos^2 z + \sin^2 z) + 2E_A E_B \cos z \\ = A^2 (\cos^2 \theta + \sin^2 \theta) \end{aligned} \quad (34)$$

or

$$A^2 = E_A^2 + E_B^2 + 2E_A E_B \cos z \quad (35)$$

Substituting equations (32) and (33) into equation (31),

$$y = A \cos \theta \sin wt - A \sin \theta \cos wt$$

which can be expressed as

$$y = A \sin(wt - \theta) \quad (36)$$

The magnitude of the E field in path A can be expressed as the magnitude of the E field in path B plus a constant:

$$\begin{aligned} E_A &= E_B + b \\ E_A^2 &= E_B^2 + 2E_A b + b^2 \end{aligned} \quad (37)$$

The intensity at meter M1 is proportional to the square of the E field magnitude, or A^2 :

$$\begin{aligned} I \sim A^2 &= 2E_B b + b^2 + 2E_B^2 + 2(E_B + b)E_B \cos z \\ I &\sim b^2 + 2E_B(b + E_B)(1 + \cos z) \\ I &\sim b^2 + 4E_B(b + E_B) \cos^2(z/2) \end{aligned}$$

If the backscattered waves were 100% conjugated, C2 would read 0 and C1 would read 100% of the energy in the backscattered wave. Since the waves will not be 100% conjugated, there will be an unconjugated, uncorrelated portion of backscattered energy (9:141). This term can be treated as random, incoherent noise.

By the symmetry of the two paths, half of the noise will be at detector M1 and half will appear at detector M2. If M2 reads only noise energy, then the total noise in the system is given by $2(M2)$. The total energy in the system is given by the sum of the two meter readings:

$$E_{\text{total}} = M1 + M2$$

Thus, the percentage of the backscattered energy consisting of noise is given by

$$E_{\text{noise}}/E_{\text{total}} = 2(M2)/(M1+M2)$$

From this, the percentage of energy which is phase conjugated is given by

$$x = 1 - [2(M2)/ (M1 + M2)] \quad (30)$$

Equation (30) represents the "reversal parameter", or amount of energy which is phase-conjugated by the SBS process.

This equation was derived for a 50% beam splitter in the interferometer. For a beam splitter of some other reflectivity, the derivation becomes more involved.

Derivation for Arbitrary Beam Splitter Reflectivity

For a beam splitter of arbitrary reflectivity, the symmetry of the two paths no longer exists. For this general case, the electric field vectors must be used to find the intensity values at meters M1 and M2. Let

$$y_A = E_A \sin wt$$

$$y_B = E_B \sin (wt - z)$$

$$y = E_A \sin wt + E_B \sin wt \cos z - E_B \cos wt \sin z$$

As figure B.4 shows, the wave traveling on path A is π out of phase from the wave traveling path B. This phase shift arises from the single reflection off the front of the beam splitter for path A. Due to this π phase shift, the two waves will destructively interfere and completely cancel each other at meter 2.

At meter 1, the two waves will constructively interfere. The wave traveling path A will undergo a phase shift of 2π due to the two reflections from the front surface of the beam splitter (one going forward and one in the reverse direction). The wave traveling path B will have no phase shift, so the two waves will add constructively at detector M1. Figure B.5 illustrates this.

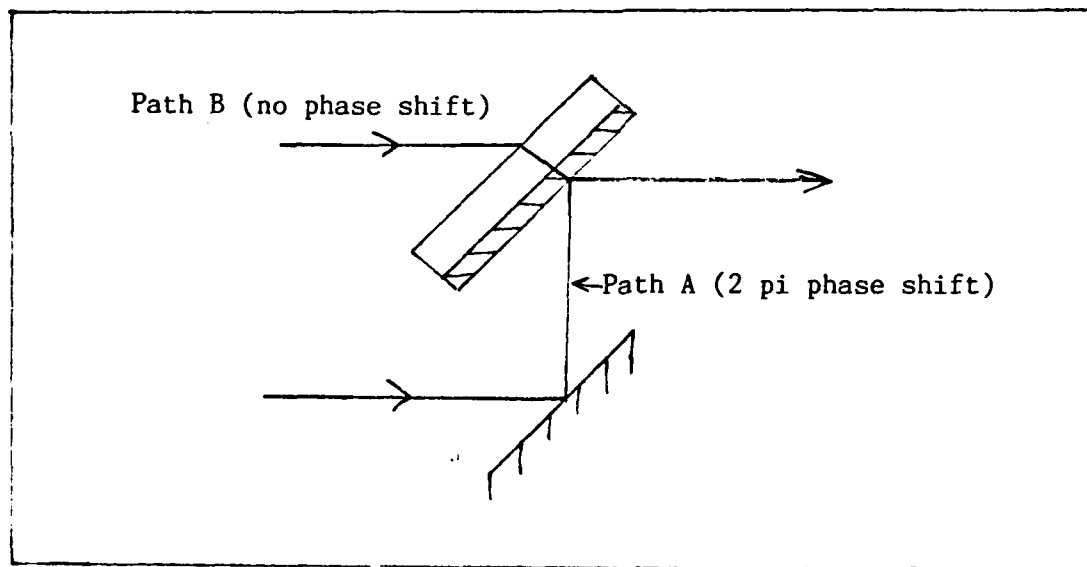


Figure B.5 Phase Shift Between Paths Going to Meter M1

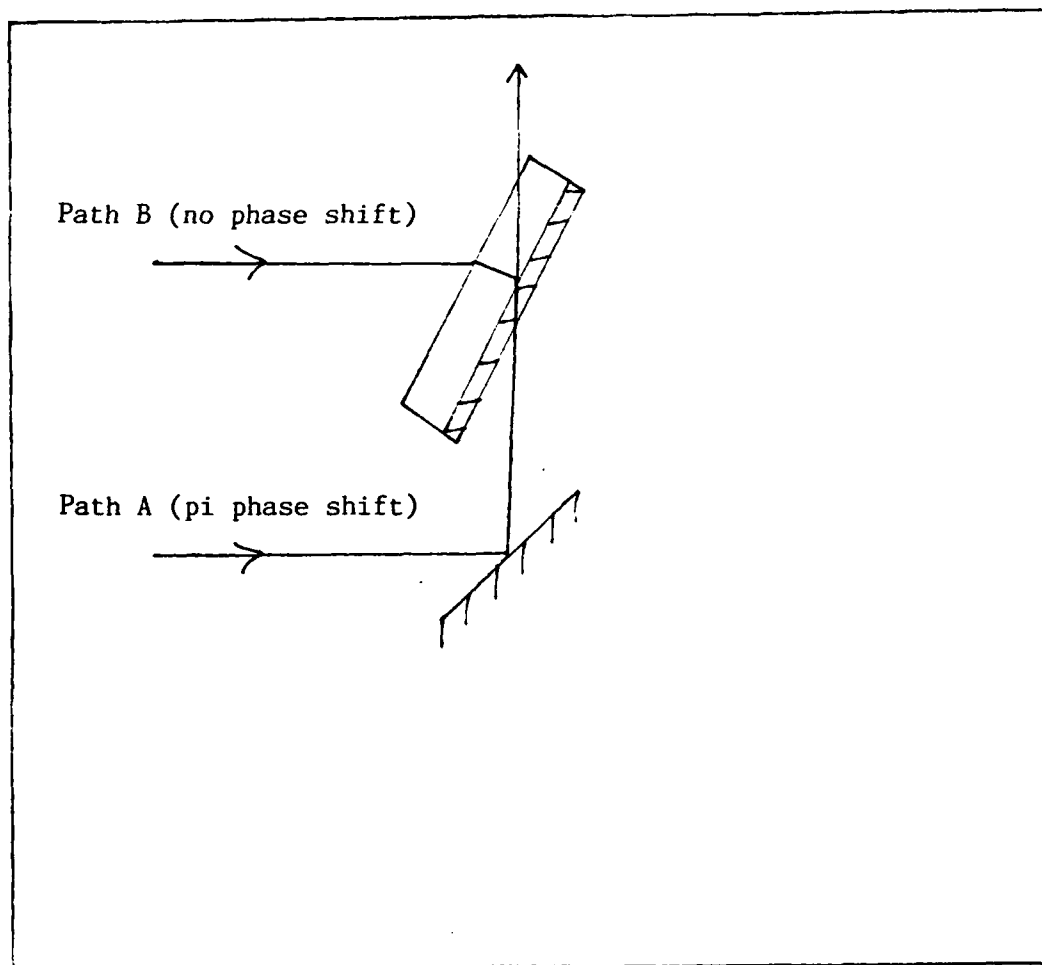


Figure B.4 Phase Shift Between Paths Going to Meter M2

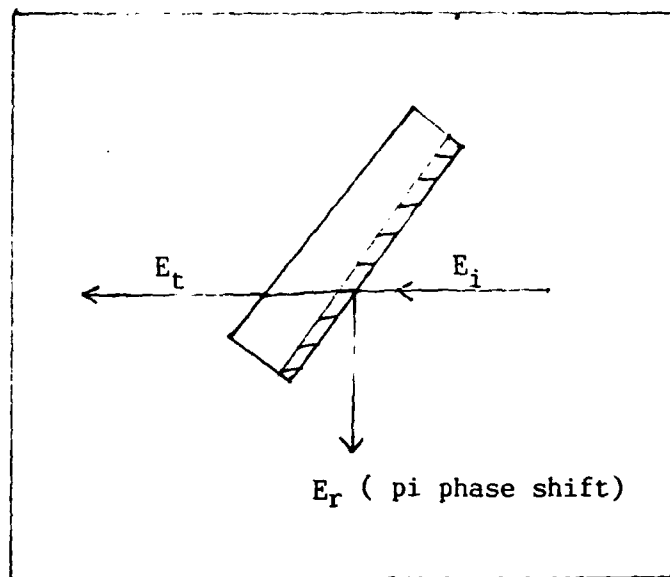


Figure B.2 First Surface Reflection
from Beam Splitter

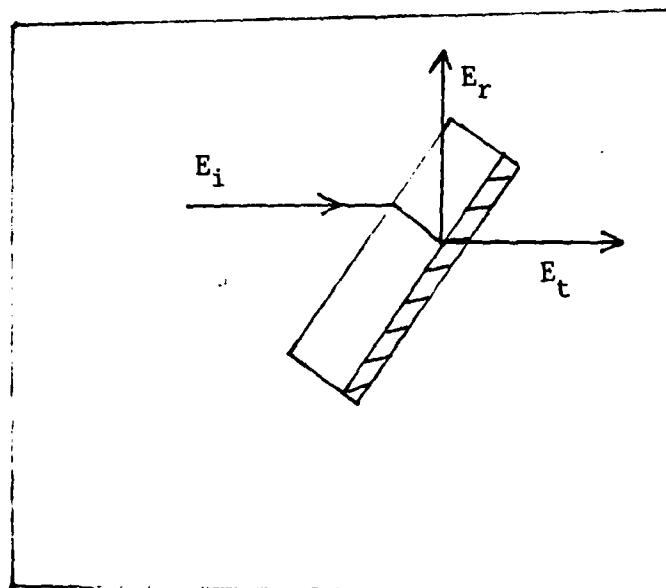


Figure B.3 Second Surface Reflection
from Beam Splitter

Appendix B: Derivation of Interferometer Method for
Measuring Conjugation Quality

The method of using a Michelson interferometer to measure the quality of conjugation in the backscattered beam will be derived here. The source for this measurement technique is reference (9). Figure B.1 shows the set-up of the interferometer used in this thesis experiment.

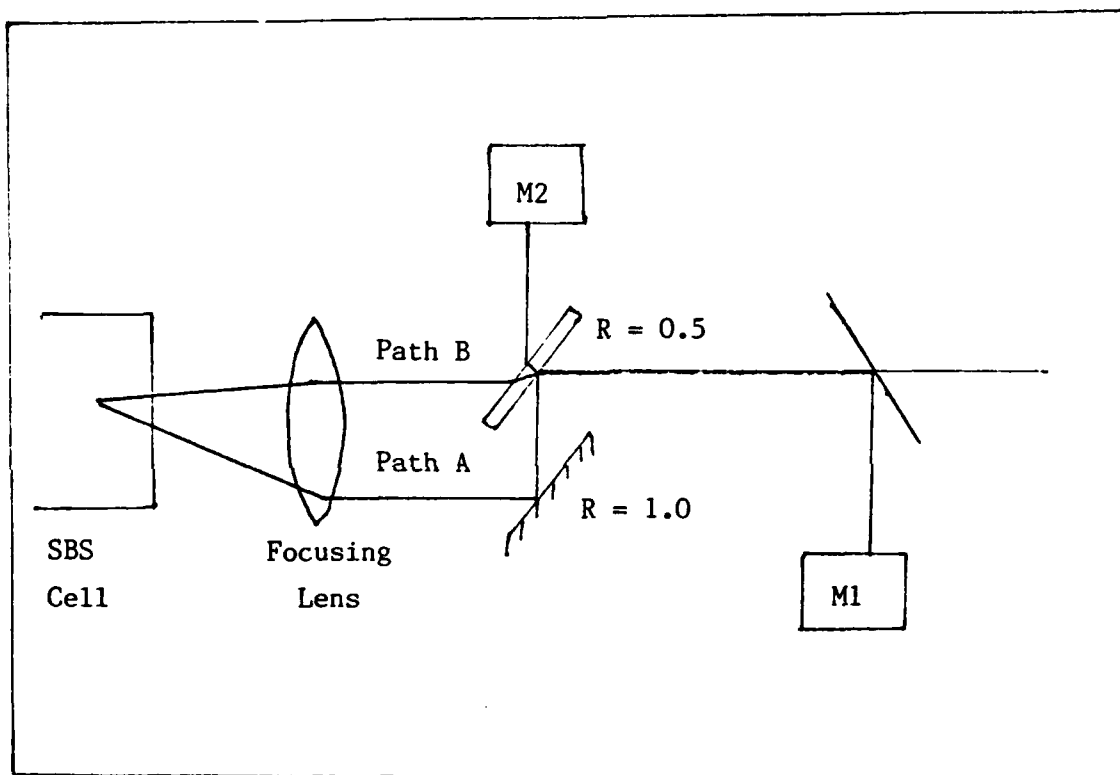


Figure B.1 Interferometer Used for Measuring Phase Conjugation Quality

First, the nature of the reflections inside the beamsplitter must be determined. Referring to fig. B.2, a π phase shift occurs between E_i and E_r , since $n_i < n_t$. No phase shift occurs between E_i and E_t (16:513).

In the case of figure B.3, no phase shift occurs between any of the three waves, since $n_i > n_t$.

The varying reflectivity of the beam splitters causes the energy readings on the EG&G meter to change with changing polarization angle. To correct the meter reading for this, the energy values can be multiplied by a correction factor $R(0)/R(x)$, where x = polarization angle. The values of this correction factor for various polarization angles appear in table III.

Table III
Energy Meter Correction Factor vs Polarization Angle of Incident Light

Polarization Angle (degrees)	Correction Factor
0	1.000
10	0.727
20	0.444
30	0.276
40	0.186
50	0.140
60	0.113
70	0.098
80	0.090
90	0.088

To determine the intensity of the reflected radiation, each component of the E field must be multiplied by its associated reflectivity and squared:

$$I_{\text{refl}} = I_o R_s \cos^2 \theta + I_o R_p \cos^2 \theta \quad (28)$$

$$I_{\text{refl}}/I_o = R_s \cos^2 \theta + R_p \cos^2 \theta \quad (29)$$

Equation (29) gives the reflectivity of the beamsplitter at a particular polarization angle. Using this equation, the calculations of beam splitter reflectivity vs polarization angle appear in Table II.

Table II
Beam Splitter Reflectivity vs Polarization Angle of Incident Light

Polarization Angle (Degrees)	Reflectivity
0	0.008
10	0.011
20	0.018
30	0.029
40	0.043
50	0.057
60	0.071
70	0.082
80	0.089
90	0.091

Appendix A: Beam Splitter Reflectivity

The reflectivity of the beam splitters in the experimental setup varies with the polarization angle of the incoming light. For s-polarization (vertical), $R_s = 0.09$. For p-polarization, $R_p = 0.008$ (13:11). Any polarization angle, other than horizontal or vertical, is a combination of s and p polarization.

Light which is polarized at an angle θ may be broken up into two orthogonal components: one of s-polarization and one of p-polarization.

$$E_s = E_o \cos\theta \quad (26)$$

$$E_p = E_o \sin\theta \quad (27)$$

Figure A.1 shows this.

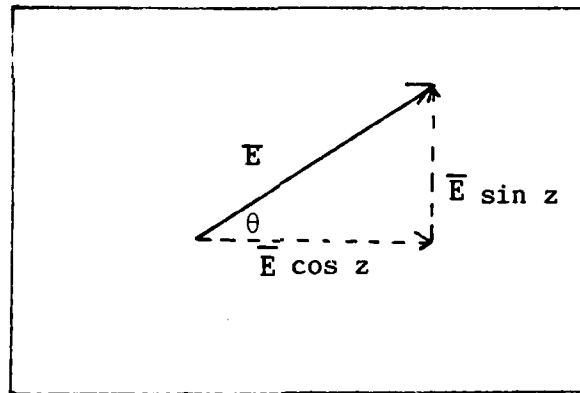


Figure A.1 Orthogonal Polarization Components

Each component of the E field has an amplitude reflectance r_p or r_s associated with it, where

$$R_p = (r_p)^2$$

$$R_s = (r_s)^2$$

splitter in the interferometer would also simplify the necessary calculations and eliminate the complex derivation for the reversal parameter equation found at the end of Appendix B.

The experiment would be worth re-working, since knowledge of the fraction of the retro pulse which is phase-conjugated would provide information about the degree of aberration correction which is possible. If only a small percentage of the backscattered energy is phase-conjugated, this would explain the often incomplete degree of distortion correction.

"information" needed to correct for the diffraction was lost. In order to provide a higher degree of correction, the cell has to collect more of the diffraction pattern.

One way to do this would be to use a tapered waveguide inside the cell. The waveguide would have a fairly large entrance aperture, then taper down to a narrow diameter. The tapering angle would have to be such that a ray entering the waveguide axially would undergo total internal reflection. In this way, the waveguide would collect more of the diffraction pattern, then guide the collected energy down to a small region in the cell. All parts of the diffraction pattern in the waveguide would be SBS-reflected, providing better correction for the apertures. It would be interesting to see if this tapered capillary increased the SBS reflectivity and the correction for the apertures in the beam. If this turned out to be true, SBS could be a practicle way to compensate for such things as a cracked solid-state laser amplifier rod, or the presence of any type of aperture which causes noticeable diffraction in the beam.

Investigation of Cornu Pseudodepolarizer. The Cornu Pseudodepolarizer could possibly have lowered the SBS threshold. It appeared to do so, but the energy meters were not sensitive enough to accurately determine this. Using more sensitive meters to measure the retro pulse energy, the energy going into the cell could be increased from zero to the point where SBS first becomes detectable - the threshold point.

This technique could be repeated with the CPD in the beam. The increased reflectivities of the beam splitters would also have to be known precisely in order to correct the meter readings. A comparison of the input energy required to produce SBS with and without the depolarizer would show if it has any effect on the SBS threshold.

Interferometer. The interferometer measurements to determine phase-conjugation quality could be repeated in order to get more accurate, usable results. With a pair of sensitive, calibrated energy meters to measure the retro pulse energies, many of the problems encountered in this experiment would be eliminated. Using a 50% beam

occurred in the cell. The gas bubbles formed by the breakdown were trapped in the capillary, effectively blocking it.

Correction for Birefringent Aberrators. Aberrators which changed the polarization of the beam had no effect on the SBS return. The Cornu Pseudodepolarizer, which provided 80% depolarization of the beam, did not degrade the SBS return. Apparently, enough residual polarization remained in the beam to drive the SBS process.

The quarter-wave plate, which rotated a portion of the beam's polarization, did not affect the SBS return at all.

Correction for Focusing Aberrators. The SBS return compensated for aberrators which had a focusing effect on the beam. The cylindrical lens telescope had no effect on the SBS return. The SBS return compensated for the presence of the single cylindrical lens, which introduced phase curvature and divergence into the beam. This showed that SBS could correct for an asymmetrically focusing lens, or anything else which caused phase-front curvature of the beam.

Correction for 1-D and 2-D Apertures. The collected data indicated some degree of correction for distortion caused by 1-D and 2-D apertures. The spatial distribution of the SBS retro pulse showed less spatial modulation than the spatial distribution of the mirror retro pulse showed.

Recommendations for Further Study

This final section contains recommendations for further study to answer some questions left by this thesis. These suggestions include using a tapered waveguide SBS cell for aperture distortion correction, further investigation of the Cornu Pseudodepolarizer, and a new experiment using the interferometer to measure phase-conjugation quality.

Tapered-Waveguide SBS Cell. One reason why the capillary SBS cell could not provide complete correction for the aperture-induced distortion is that part of the diffraction pattern from the apertures missed the narrow capillary entrance, which meant that part of the

Included the large screen, the stack of seven apertures, the 50% beam splitter, and the 250 mm cylindrical lens. The data from these measurements proved to be very erratic; it was very inconsistent and had no discernible pattern. When the energy readings were put into the equation for the reversal parameter, the answer often came out greater than one or negative.

A major problem with the configuration of the interferometer was trying to align both of the beams from the interferometer into the capillary of the SBS cell. The two beams had to remain parallel, so that the lens would focus them to the same point at the SBS cell. Getting both of the beams to stay within the narrow acceptance angle of the capillary turned into a laborious trial-and-error alignment process. No SBS occurred until both of the beams remained confined within the capillary. Once SBS was achieved, blocking either of the beams would prevent the SBS from occurring. This showed that neither beam possessed sufficient intensity by itself to reach SBS threshold.

The unproductive performance of the interferometer meant a major failure in the experiment. Lack of knowledge of how much of the backscattered pulse was being phase-conjugated limited the number of conclusions which could be drawn about the ability of phase-conjugation process to correct for aberrations.

Conclusions

This section contains conclusions drawn from the data and possible explanations for observed phenomena. If the collected data did not merit a firm conclusion, possibilities as to why the observation happened are discussed.

SBS Cell Performance. Due to the increased interaction length provided by the capillary waveguide, the capillary SBS cell required a much lower peak-power input to reach SBS threshold than the non-capillary cell needed. This allowed the capillary cell to reach SBS threshold with long-pulse input; the non-capillary cell needed the higher peak power provided by Q-switched input.

The capillary SBS cell did not perform well if plasma breakdown

two different paths for the light to travel to the SBS cell. When the backscattered light in the two paths recombines at the beam splitter, the two paths interfere either constructively or destructively.

Any length difference between the two paths is compensated for by the phase-conjugate wave (see Chapter II). Due to a π phase shift between the two reflections, the two paths interfere destructively going to meter M2. Thus, all of the backscattered energy going to meter M2 which is phase-conjugated will be cancelled out. The only energy reaching M2 will be the incoherent portion of the backscattered energy - the unconjugated "noise".

No net phase shift occurs between the two paths going to meter M1. Thus, the phase-conjugated portion of the backscattered energy in the two paths going to meter M1 recombines constructively. If the beam splitter divides the beam into two equal parts, the noise portion of the backscattered energy will be equally present at M1 and M2. The fraction of the backscattered energy which is phase-conjugated, known as the "reversal parameter", is given by

$$x = 1 - [2(M2) / (M1 + M2)] \quad (25)$$

where

M1 = energy at meter M1

M2 = energy at meter M2

For a more complete theoretical description of the interferometer and derivation of the above equation, see Appendix B.

A suitable 50% beam splitter was not available for the experiment, so an $R = 0.7$ beam splitter was substituted. This greatly complicated the derivation of the equation for the reversal parameter, as given in the second section of Appendix B.

The two EG&G radiometers were used for meters M1 and M2. They both had to be operated on their most sensitive scales, which created the previously-discussed problems of balancing the meters and of accuracy.

Data was taken with several different aberrators in place. These

$$\begin{aligned}
 I &\sim b^2 + 4E_A E_B \cos^2(z/2) \\
 I &\sim b^2 + 4RT \cos^2(z/2)
 \end{aligned}
 \tag{38}$$

where

R = reflectivity of beam splitter

T = transmission of beam splitter

The b^2 term is a function of the energy difference between path A and path B. Assuming that the input field = 1, the path A field has a value of $(\sqrt{R})^2$ and the path B field has a value of $(\sqrt{T})^2$. This means that the energy difference between the two paths is

$$b^2 = (R - T)^2$$

For channel 2 (going to meter M2), the b^2 term = 0. This comes from the fact that path A and path B each go through one reflection and one transmission of the beam splitter, giving them equal intensities. Since all phase-conjugated energy going to M2 is cancelled out by the π phase shift between the two paths, only noise will remain at M2. Due to the incoherence of the noise, the average value of the $\cos^2(z/2)$ term will equal 1/2. Thus, from equation (38), the M2 meter reading will equal 2RT (assuming that all of the backscattered energy is phase-conjugated).

Since this is an interferometer, the well-known equation for fringe visibility

$$V = (I_{\max} - I_{\min}) / (I_{\max} + I_{\min}) \tag{39}$$

applies. The fringes would appear as in figure B.6.

The meter M1 reading is given by

$$k_1 M1 = I_{in} [b^2 + 4RT \int \cos^2(z/2) dz] \tag{40}$$

The meter M2 reading is given by

$$k_2 M2 = I_{in} [4RT \int \cos^2(z/2) dz] \tag{41}$$

where k_1 and k_2 are constants to calibrate the meter reading to mJ, and I_{in} is input intensity. Let

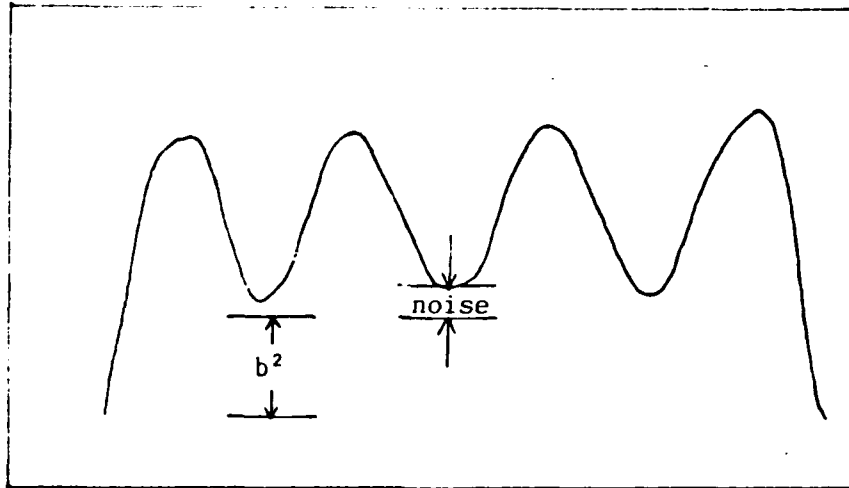


Figure B.6 Fringes at Meter M1 Resulting from Interferometer

$$M1^* = k_1 M1 / I_{in} - b^2$$

$$M2^* = k_2 M2 / I_{in}$$

where b^2 is defined as $I_{in}(R - T)^2$.

$M1^*$ represents constructive interference of the two channels from the phase-conjugate portion of the retro pulse, plus incoherent noise. $M2^*$ represents only incoherent noise. After the b^2 term has been subtracted off (it is a "bias" term and supplies no useful information), the fringes appear as in figure B.7.

The form of $M1^*$ and $M2^*$ given by equations (40) and (41) shows that the same noise term occurs in each. The minimum value for $M1^*$ is just the noise term

$$I_{in} 4RT \int \cos^2(z/2) dz$$

The minimum and the maximum value for $M2^*$ is this same noise term. Thus, for the interferometer, I_{max} is the value of $M1^*$ due to constructive interference. I_{min} is the noise , given by $M2^*$. For the

visibility of fringes,

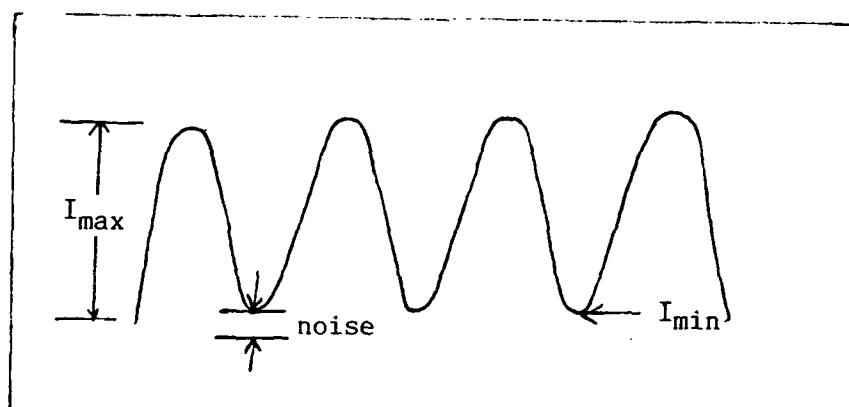


Figure B.7 Interferometer Fringes with Bias Removed

$$V = (M1^* - M2^*) / (M1^* + M2^*)$$

$$= 1 - [2M2^* / (M1^* + M2^*)]$$

or

$$V = \frac{1 - 2k_2 M2 / I_{in}}{(k_1 M1 / I_{in}) + (K_2 M2 / I_{in}) - (R - T)^2} \quad (42)$$

where

k_1, k_2 = meter calibration constants

$M1$ = meter 1 reading

$M2$ = meter 2 reading

I_{in} = input intensity

R, T = reflectance and transmission of beam splitter

Equation (42) gives the percentage of backscattered energy which is phase-conjugated. If $R = T$, this equation reduces to the form of equation (30), which gives the reversal parameter for the 50% beam splitter case.

Bibliography

1. Baldwin, George C. An Introduction to Nonlinear Optics. New York: Plenum Press, 1969.
2. Basov, N.G. et al. "Inversion of Wavefront in SMBS of a Polarized Pump," JETP Letters, 28: 197-200 (20 August 1978).
3. Basov, N.G. et al. "Small Signal Wavefront Reversal in Nonthreshold Reflection from a Brillouin Mirror," Soviet Journal of Quantum Electronics, 6: 237-239 (Feb 1979).
4. Basov, N.G. et al. "Phase Fluctuations of the Stokes Wave Produced as a Result of Stimulated Scattering of Light," JETP Letters, 31: 645-649 (5 June 1980).
5. Basov, N.G. et al. "Laser Interferometer with Wavefront Reversing Mirrors," Soviet Physics JETP, 52: 847-851 (Nov 1980).
6. Bepalov, V.I. "Observation of Transient Field Oscillations in the Radiation of Stimulated Mandel'shtam-Brillouin Scattering," JETP Letters, 31: 630-633 (5 June 1980).
7. Fisher, Robert A. Telephone interview. Los Alamos National Laboratory, Los Alamos, N.M., 28 September, 1984.
8. Grasyuk, A.Z. et al. "Influence of Spectral Linewidth of Exciting Radiation on the Gain in Stimulated Scattering," JETP Letters, 16: 166-169 (20 Aug 1972).
9. Hellwarth, R.W. in Optical Phase Conjugation, edited by Robert A. Fisher. New York: Academic Press, 1983.
10. Hellwarth, R.W. "Optical Beam Phase Conjugation by Stimulated Backscattering," Optical Engineering, 21: 257-261 (March/April 1982).
11. Hon, David T. "Applications of Wavefront Reversal by Stimulated Brillouin Scattering," Optical Engineering, 21: 252-261 (March/April 1982).
12. Jenkins, Francis A. and White, Harvey E. Fundamentals of Optics (Third Edition). New York: McGraw-Hill Book Company, 1957.
13. Jensen, S.M. and Hellwarth, R.W. "Observation of the Time-Reversed Replica of a Monochromatic Optical Wave," Applied Physics Letters, 32: 166-168 (1 February 1978).
14. Kaiser, W. and Maier, M. Laser Handbook, edited by F.T. Arrechi and E.O. Schultz-Dubois. New York: North-Holland Publishing Company, 1972.

15. Mays, R. and Lysiak, R.J. "Phase Conjugated Wavefronts by Stimulated Brillouin and Raman Scattering," Optics Communications, 31: 89-92 (October 1979).
16. Mays, R. and Lysiak, R.J. "Observations of Wavefront Reproduction by Stimulated Brillouin Scattering as a Function of Pump Power and Waveguide Dimensions," Optics Communications, 32: 334-337 (January 1980).
17. Melles Griot. Optics Guide 2, 1981 edition
18. Nosach, O.Y. et al. "Cancellation of Phase Distortions in an Amplifying Medium with a Brillouin Mirror," JETP Letters, 16: 435-438 (5 December 1972).
19. O'Meara, M. "Compensation of Laser Amplifier Trains with Nonlinear Conjugation Techniques," Optical Engineering, 21: 243-251 (March/April 1982).
20. Papernyl, S.B. et al. "Competition Between Stimulated Scattering and Optical Breakdown in Argon," Soviet Journal of Quantum Electronics, 13: 293-297 (March 1983).
21. Pepper, David M. "Nonlinear Optical Phase Conjugation," Optical Engineering, 21: 155-159 (March/April 1982).
22. Pilipetskii, N.F. et al. "Angular Distribution of the Noise Component of Light Scattered in a Stimulated Process," Soviet Journal of Quantum Electronics, 13: 1312-1316 (October 1983).
23. Shen, Y.R. in Light Scattering in Solids, edited by M. Cardona. New York: Springer-Verlag, 1975.
24. Sidorovich, V.G. "Theory of the Brillouin Mirror," Soviet Physics Technical Physics, 21: 1270-1274 (October 1976).
25. Slatkine, Michael A. et al. "Efficient Phase Conjugation of an Ultraviolet XeF Laser Beam by Stimulated Brillouin Scattering," Optics Letters, 7: 108-110 (March 1982).
26. Vasil'ev, M.V. "Recording of Phase Fluctuations of Stimulated Scattered Light," JETP Letters, 31: 634-638 (5 June 1980).
27. Verdeyen, Joseph T. Laser Electronics. Englewood Cliffs, N.J.: Prentice-Hall, Inc., 1981.
28. Wang, Victor and Guiliano, C.R. "Correction of Phase Aberrations via SBS," Optics Letters, 2: 4-6 (Jan 1978).
29. Williams, William E. et al. "Optical Switching and n_2 measurements in CS_2 ," Optics Communications, 50: 256-260 (15 June 1984).

30. Zel'Dovich, B. Ya. et al. "Connection Between the Wavefronts of the Reflected and Exciting Light in Stimulated Mandel'Shtam-Brillouin Scattering," JETP Letters, 15: 109-112 (5 February 1972).

31. Zel'Dovich, B. Ya. et al. "Phase Conjugation in Stimulated Scattering," Soviet Physics USP, 25: 713-734 (October 1982).

VITA

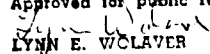
Thomas Frederick Lowum was born on 1 August, 1961 in Indianapolis, Indiana. He graduated from Cicero High School in North Syracuse, New York in 1979. Following this, he attended the Cornell University School of Engineering, from which which he received a Bachelor of Science Degree in May of 1983. Upon graduation, he was commissioned in the USAF as a distinguished graduate of the AFROTC program and entered the School of Engineering, Air Force Institute of Technology , in June 1983.

Permanent Address: 5931 Smith Rd
N. Syracuse, NY 13212

UNCLASSIFIED

SECURITY CLASSIFICATION OF THIS PAGE

REPORT DOCUMENTATION PAGE

REPORT SECURITY CLASSIFICATION UNCLASSIFIED			1b. RESTRICTIVE MARKINGS	
2a. SECURITY CLASSIFICATION AUTHORITY			3. DISTRIBUTION/AVAILABILITY OF REPORT Approved for public release; distribution unlimited	
2b. DECLASSIFICATION/DOWNGRADING SCHEDULE				
4. PERFORMING ORGANIZATION REPORT NUMBER(S) AFIT/GE/PH/84D-1			5. MONITORING ORGANIZATION REPORT NUMBER(S)	
6a. NAME OF PERFORMING ORGANIZATION School of Engineering		6b. OFFICE SYMBOL (If applicable) AFIT/ENP	7a. NAME OF MONITORING ORGANIZATION	
6c. ADDRESS (City, State and ZIP Code) Air Force Institute of Technology Wright-Patterson AFB, Ohio 45433			7b. ADDRESS (City, State and ZIP Code)	
8a. NAME OF FUNDING/SPONSORING ORGANIZATION Avionics Laboratory		8b. OFFICE SYMBOL (If applicable) AFWAL/AADO	9. PROCUREMENT INSTRUMENT IDENTIFICATION NUMBER	
8c. ADDRESS (City, State and ZIP Code) AFWAL/AADO Bldg 22B Wright-Patterson AFB, Ohio 45433			10. SOURCE OF FUNDING NOS.	
11. TITLE (Include Security Classification) see box 19			PROGRAM ELEMENT NO. 62204F	PROJECT NO. 2001
			TASK NO. 05	WORK UNIT NO. 09
12. PERSONAL AUTHOR(S) Thomas F. Lowum, B.S., 2nd Lt., USAF				
13a. TYPE OF REPORT MS Thesis		13b. TIME COVERED FROM _____ TO _____	14. DATE OF REPORT (Yr., Mo., Day) 1984 December	
15. PAGE COUNT 89				
16. SUPPLEMENTARY NOTATION				
17. COSATI CODES			18. SUBJECT TERMS (Continue on reverse if necessary and identify by block number)	
FIELD	GROUP	SUB. GR.	<input checked="" type="checkbox"/> Optics Optical Phaseconjugation, Optical Retroreflection Electromagnetic Wave Reflection	
20	06			
19. ABSTRACT (Continue on reverse if necessary and identify by block number)				
<p>Title: STIMULATED BRILLOUIN SCATTERING REFLECTIVITY IN THE PRESENCE OF VARIOUS ABERRATORS</p> <p>Thesis Chairman: Dr. W.B. Roh</p> <p style="text-align: right;">Approved for public release: IAW AFR 190-17.  LYNN E. WCLAYER Dean for Research and Professional Development Air Force Institute of Technology (AFIT) Wright-Patterson AFB OH 45433</p>				
20. DISTRIBUTION/AVAILABILITY OF ABSTRACT UNCLASSIFIED/UNLIMITED <input checked="" type="checkbox"/> SAME AS RPT. <input type="checkbox"/> DTIC USERS <input type="checkbox"/>			21. ABSTRACT SECURITY CLASSIFICATION UNCLASSIFIED	
22a. NAME OF RESPONSIBLE INDIVIDUAL Dr. W.B. Roh			22b. TELEPHONE NUMBER (Include Area Code) 513-255-4877	22c. OFFICE SYMBOL AFIT/ENP

DD FORM 1473, 83 APR

EDITION OF 1 JAN 73 IS OBSOLETE

UNCLASSIFIED
SECURITY CLASSIFICATION OF THIS PAGE

The phase-conjugate nature of a light wave reflected by Stimulated Brillouin Scattering was studied to determine the amount of compensation provided by SBS for aberrations in the system. The SBS medium used was CS_2 liquid contained in a cylindrical glass cell. Two different types of cell were used: one with a narrow capillary waveguide inside it and another without any type of waveguide.

The ability of SBS to correct for aberrators which change the polarization of the beam, focus the beam, or diffract the beam was studied. These aberrators included a sapphire quarter-wave plate, a Cornu Pseudodepolarizer, a cylindrical lens telescope, a single cylindrical lens, overlapping microscope slides (one-dimensional apertures), and a piece of wire mesh (two-dimensional apertures).

The SBS return compensated either partially or completely for all of the aberrators tested. The results also indicated that the cell with the waveguide had a much lower SBS threshold than the other cell.

Key words include:

END

FILMED

5-85

DTIC